International Review of
Chemical Engineering
Rapid Communications
(IRECHE)

Contents

Praise Worthy Prize

Praise Worthy Prize

International Review of Chemical Engineering (I.RE.CH.E.), Vol. 6, N. 3
ISSN 2035-1755 *May 2014*

Investigating of Erosion Corrosion in Horizontal Steel Pipes with Slurry Seawater Flow

M. El-Zebda, M. Shehadeh, I. Hassan

Abstract – *Erosion corrosion is main problem in marine structures, such as offshore pipelines and a ship's propeller churning in the ocean. Understanding the failure mechanism due to erosion helps in the review of pipeline design. This paper concerns with studying the behavior of A106 carbon-steel pipes working in two different erosive environments (i.e. plain and slurry seawater). Series of laboratory experiments are carried out to investigate the rates of iron losses due to both flow rate variations and sand concentration variations. The flow rate is controlled to cover both the laminar and turbulent flow regimes. The sand concentration varies from null to 9 g/l. The relationship between the rate of corrosion rate and flow rate at different levels of contamination is investigated. A regression equation is developed to describe the relationship of different erosion-corrosion rate at laminar and turbulent flow regimes along with different sand contamination levels.*

Keywords*: Erosion-Corrosion, Turbulent, Pipeline Corrosion, Slurry, Seawater*

I. Introduction

The National Energy Board [1] estimated that the ultimate volume of crude bitumen in place is to be some 400 billion cubic meters. With the continuously growing demand in oil consumption, conventional energy sources are suffering from depletion.

The dependency on the oil sands, as a new source of energy, will be increasing rapidly to compensate the difference in the future global oil production. Hydro transport of Oil sand is a method of transporting oil sand and preparing it for upstream processing all at the same time. The hydro transport process, oil sands and water are mixed together to make a slurry. This slurry is transported via pipeline from the mine to a bitumen extraction facility. There is no doubt that oil sand hydro transport is a much less expensive and more flexible way to move oil sand than the old method. However, erosion-corrosion and their synergism, erosion corrosion (E-C) have constituted an essential threat to the integrity of the oil sand slurry hydro transport system [2], [3]. Erosion corrosion is acceleration in the rate of corrosion attack in metal due to the Relative motion of the environment and the metal surface [4]. For example, in oil sand slurry, the presence of water and oxygen, combined with the salts, causes corrosion to the carbon steel pipes, which is accelerated by the flowing slurry and the solid sand particles.

The synergistic effects of corrosion and erosion can generate material loss much greater than that caused by individually [5], [6]. Development of the effective technique for prevention of Hydro transport pipe E-C has been identified as one of the highest profitable research priorities in oil sand industry [2].

Understanding of E-C of metals is complex, and considerable work is required to determine the interaction of affecting parameters and, furthermore, the synergism of corrosion and erosion [7]. One of the most challenging pipelines system operations is early detect for any abnormal behaviors that may lead to catastrophic accidents.

The most crucial factor in pipeline operating system is the control of the pipe's corrosion. During the operation of the pipeline system, the system process may contain a corrosive flow (e.g. seawater) or operates in various velocities (e.g. laminar or turbulent). So all of this can generate a suitable zone for the birth of erosion-corrosion and many huge consecutive problems can be occurred. In addition, a fault can be very costly in terms of production loss. Online monitoring for pipeline erosion-corrosion is an important task for early detection for abnormal situation that may lead to catastrophic accident [8].

The overall objective of this paper studies the fundamentals of E-C of water pipe steel under different conditions that might be relevant to oil sand slurry transportation. The parametric effects, including different slurry seawater flow velocities (i.e. Reynolds numbers) and sand concentrations on E-C of pipe steel are investigated by weight loss technique.

II. Experimental and Procedures

Identifying the damage behavior by E-C in the tested pipe is the main objective of this study. Reaching this target is achieved by identifying the tested pipes specifications and behavior in different mediums at various velocities.

Manuscript received and revised April 2014, accepted May 2014

Experimental apparatus is shown in Fig. 1 and procedures are described in following sections. Two series of experiments are carried out; the first series of experiments for studying the E-C rate in the pipes by using plain seawater and the second series experiments expose the tested pipes to a flow of seawater with solid particles (sand).

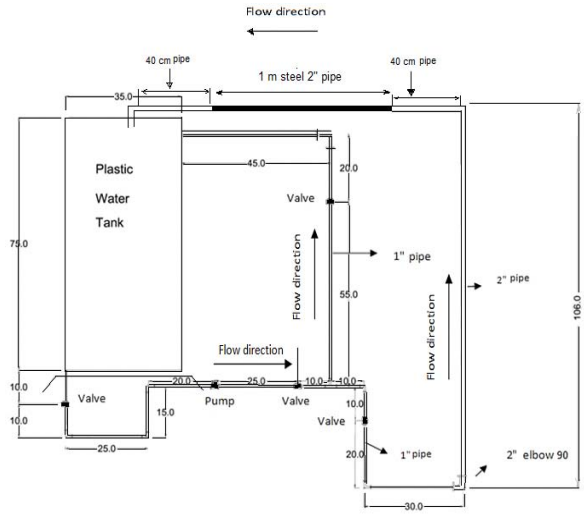

Fig. 1. Schematic experimental system

Many steps had been considered before starting experiments, firstly: choosing the material of the tested specimen, secondly: assembling the experimental system apparatus, thirdly determining the system velocities. All experiments were carried out at room temperature using eight seamless pipes of steel class B (A106). The seamless pipe has dimensions of 52 mm internal diameter, 4 mm wall thickness and 1 m length. Hence, Pipe of class B (A106) is widely used in fields of offshore platforms which proposed as more exposed material for erosion-corrosion phenomena.

The E-C rates were determined for flow regimes ranging from laminar, i.e. Re < 2300, up to turbulent flow regimes of seawater at different levels of sand contamination. The Reynolds number calculations were based on the pipe inner diameter.

The seawater density and dynamic viscosity were taken as 1025 kg/m^3 and 0.0011 kg/ms, respectively [9]. Seawater was prepared at the laboratory by dissolving 35 grams of salt in each liter of water [10]. However, direct usage of seawater is not recommended as it can contain uncontrollable concentrations of solid particles, which can also have harmful effects to the system.

Total weight loss of iron was measured every 1800 second for a period of 10800 second of whole system operation.

The weight loss was measured for plain seawater and sand-contaminated seawater with sand concentrations of 3 g/l, 6 g/l and 9 g/l for eight different flow velocities (i.e. Reynolds number), see Table I. Sand of average grain size of 300 μm was added to the prepared seawater at different concentrations.

Spectrophotometer (i.e. microprocessor-controlled, single-beam instrument for colorimetric testing) was used to measure the quantity of iron loss from the steel pipe in each sample of seawater. Also commercial iron reagent was used to determine the quantity of iron in seawater.

The E-C analyses in these experiments were carried out for the determinations of its rate in each pipe in the four different mediums and at certain velocity of the flow every three hours. A water sample of the out flowing water was collected every 1800 seconds in a clean test tube which was initially washed with distilled water.

Eight pipes were tested in four different mediums (i.e. seawater and three sand concentrations).

III. Results and Discussions

The erosion-corrosion rate was estimated from the quantity of iron loss from the carbon steel of the pipeline system. Hence, the erosion corrosion rate was calculated using Eq. (1) at all mediums for eight different velocities (i.e. Reynolds number) with 30 minute increments. Erosion-corrosion rate is commonly given by the following expression:

$$\text{Erosion-corrosion rate} = \frac{WL}{A \times T} \qquad (1)$$

where:

WL	iron loss weigh	(mg)
A	inner pipe surface area	(cm^2)
T	time	(s)

The results of calculated E-C are estimated for all cases. As an example for the results, only two results of uncontaminated and contaminated seawater of 9 g/l sand are chosen for presenting the behaviour of E-C with time, show in Figs. 2, 3, 4 and 5. Figs. 2 and 3 show a direct relationship between the E-C rate and the time for the laminar flow case with constant increment time of 1800 second in each velocity.

Figs. 4 and 5 show the same relation for the turbulent flow case. From the observation of the trends at all mediums, it is clear that the increase of erosion-corrosion rate is observed here due to the change in the flow regime from laminar to turbulent, especially for seawater with concentration of sand 9 g/l at turbulent flow.

Moreover, the increase in weight losses due to sand contamination arises due to erosion effects as described by [11].

However, for uncontaminated seawater, the increase of erosion-corrosion rate at laminar flow is lower than all other cases. Accordingly, it can be concluded that the main two parameters that effect directly the E-C rate is the flow velocity and sand concentrations which is agree with many researchers [12],[13].

From Figs. 2, 3, 4 and 5, the E-C is slightly decreased from time of 1800 second to 7200 second; thereafter the

E-C rate is almost constant. Accordingly, it can be developed regression equations for different contaminations seawater in both laminar and turbulent regimes at time of 10800 second.

The regression equation is developed here by using commercial software. For choosing the most suitable equations for laminar and turbulent cases a regression analysis to be attempted for fitting a linear model. The modeler should be first determined whether or not there is a relationship between the variables of interest.

This does not necessarily imply that one variable causes the other, but that there is some significant association between the two variables. Depending on these results, Reynolds numbers and sand concentration have been chosen.

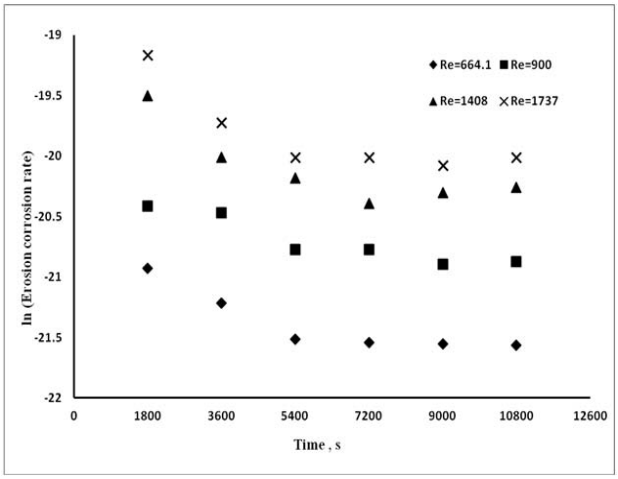

Fig. 2. Erosion corrosion rate vs time for seawater at different laminar flow

Fig. 6 clearly indicates that rabidly increase in erosion-corrosion rate by increasing the quantity of solid particles in seawater as well as increasing the flow velocity. The E-C obeyed a linear relationship with the flow velocity, as shown in Fig. 4. Accordingly, regression equations for E-C rates are proposed from the linear trends of Fig. 4:

For laminar regime:

$$LnE - C = 0.001Re + 013Sc - 21.97 \qquad (2)$$

and for turbulent regime:

$$LnE - C = 5.53\times10^{-5}\, Re + 0.08Sc - 19.73 \qquad (3)$$

where the Sc is sand concentration in g/l. The Eqs. (2) and (3) can help in prediction of the constant E-C rates based on the flow velocity and solid particle concentrations at certain time of system operations [14].

Finally, a high resolution camera was used to investigate the internal surface of all pipes after three hours of operation for each Reynolds number. The erosion of the pipe is depicted in Figs. 7 and 8 [15].

The E-C experiments and found that less standard error at 10800 second.

From Figs. 2-5 and Table I, the E-C rate has been found approximately stable starting from 10800 second which also considered as a less standard error.

Fig. 6 shows the E-C rate of iron losses and individual contributors as a function of the sand concentration and Reynolds number at certain time of 10800 second.

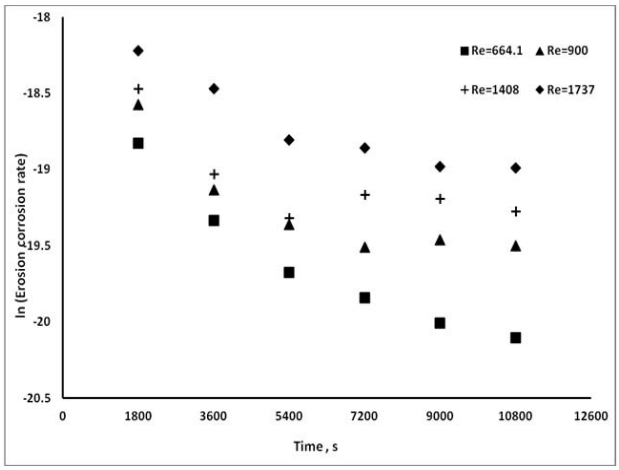

Fig. 3. Erosion corrosion rate vs time for slurry seawater(9 g/l sand) at different laminar flow

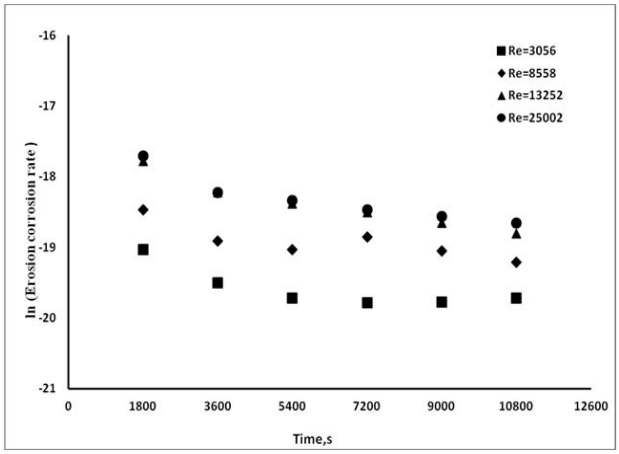

Fig. 4. Erosion corrosion rate vs time for seawater at different turbulent flow

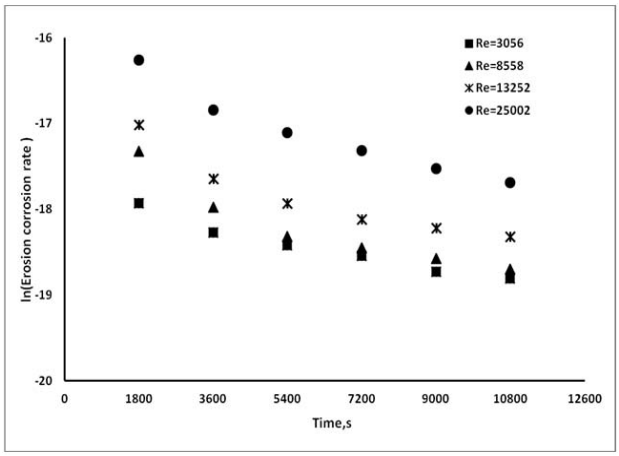

Fig. 5. Erosion corrosion rate vs time for slurry seawater (9 g/l sand) at different turbulent flow

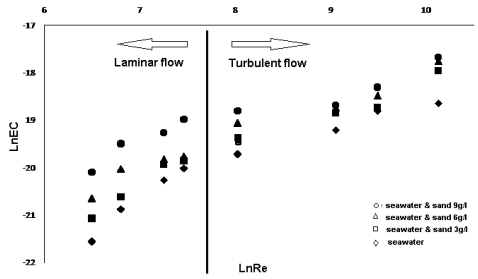

Fig. 6. Erosion Corrosion rate Vs Reynolds at 10800 second.

TABLE I
STANDARD ERROR OF REGRESSION EQUATIONS FOR LAMINAR AND TURBULENT FLOW

Time(s)	Standard error	
	Laminar	Turbulent
3600	0.23	0.228
5400	0.2	0.217
7200	0.191	0.227
9000	0.185	0.176
10800	0.218	0.138


(a) Reynolds 664


(b) Reynolds 900


(c) Reynolds 1408

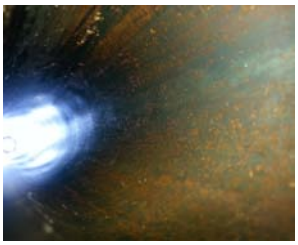
(d) Reynolds 1737

Figs. 7. Internal surface of pipes for slurry seawater at different laminar flow regime

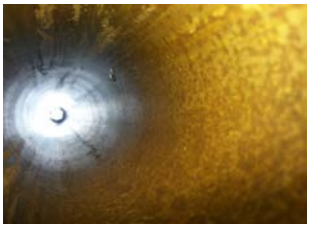
(a) Reynolds 3056

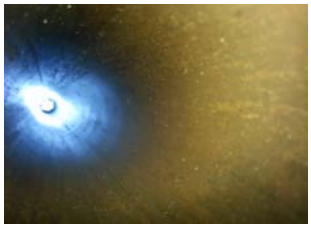
(b) Reynolds 8558

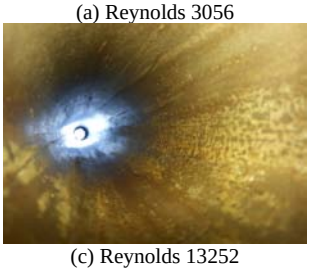
(c) Reynolds 13252

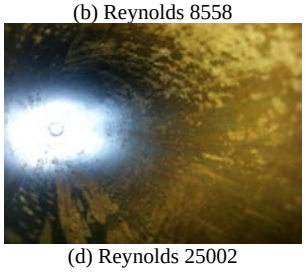
(d) Reynolds 25002

Figs. 8. Internal surface pipes for slurry seawater at different turbulent flow regime

IV. Conclusion

The effect of seawater flow rate with different sand contamination levels on erosion-corrosion rates in this work is investigated. The erosion corrosion rate increases linearly with increasing the flow velocities and sand concentrations.

Two regression equations were derived to determine the erosion-corrosion rate in laminar and turbulent regimes.

Chemical analyses can be used only as a quantitative technique to monitor and predict the E-C effects in pipeline systems.

However, further numerical and experiments investigations required on other geometries, such as large scale of pipelines, in different corrosive environments to study the qualitative as well as quantitative effect of erosion-corrosion rate and location along pipelines.

References

[1] National Energy Board, Canada's Oil Sands, *A Supply and Market (2000).*
[2] *Petroleum Technology Alliance Canada, Research Priorities (Upstream Conventional Oil & Gas), Canada (2001).*
[3] Robert J.K. Wood, Erosion–corrosion interactions and their effect on marine and offshore materials, *Wear, 261 (2006), 1012–1023.*
[4] D.D. Macdonald, G.A. Cragnolino, *Corrosion of Steam Cycle Materials (ASME Handbook 1989).*
[5] Y. Li, G.T. Burstein, I.M. Hutchings, 1995: Influence of environmental composition and electrochemical potential on the slurry erosion-corrosion of aluminum, *Wear, 181(1995), 70-79.*
[6] M.M. Stack, N. Pungwiwat, Particulate erosion–corrosion of Al in aqueous conditions: some perspectives on pH effects on the erosion–corrosion map, *Tribology International, 35(2002), 651–660.*
[7] S.S. Rajahram, T.J. Harvey, R.J.K.Wood, Erosion–corrosion resistance of engineering materials in various test conditions, *Wear, 267 (2009), 244–254.*
[8] M. Shehadeh, I. Hassan, H. Mourad, H.EL-Gamal, Monitoring Erosion Corrosion in Carbon Steel Elbow Using Acoustic Emission Technique, *30th European Conference on Acoustic Emission Testing /7th International Conference on Acoustic Emission, Granada, Spain, June (2012).*
[9] C.Q. Guo, C.H. Zhang, M.P. Paidoussis, Modification of equation of motion of fluid-conveying pipe for laminar and turbulent flow profiles, *Journal of Fluids and Structures, 26 (2010), 793-803.*
[10] F. Culkin, *The Major Constituents of Seawater, Chemical Oceanography, l (1965), 121-161.*
[11] T. Boran, 2007: Mechanistic Understanding and Effective Prevention of Erosion-corrosion of Hydrotransport Pipes in Oil Sand Slurry, *MSc. Thesis, University OF Calgary, Canada (2007).*
[12] M .R.Ansari, S. Mohammadi And M.K. Oskouei, 2012: Two-phase Gas/Liquid-Solid Flow Modeling in 90° Bends and Its Effect on Erosion, *Global Journal of researches in engineering, 12(1)(2012), 35-44.*
[13] M. Shehadeh, A.I. Shahata, M. El-Shaib and A. Osman, Numerical and Experimental Investigations of Erosion-corrosion in Carbon-steel Pipelines, *International Journal of Applied Engineering Research, 8 (11) (2013), 1217-1231.*
[14] Rajat Gupta, S.N. Singh, V. Sehadri, Prediction of uneven wear in a slurry pipeline on the basis of measurements in a pot tester, *Wear, 184 (1995), 169-178.*
[15] Md .AminulIslam, Zoheir.N.Farhat, The synergistic effect between erosion and corrosion of API pipeline in CO2 and saline medium, *Tribology International 68 (2013), 26-34.*

Authors' information

Eng. **Mohamed El-Zebda** is currently Master student at Marine Engineering Dpt., Arab Academy for Science, Technology and Maritime Transport (AASTMT), Alexandria, Egypt. He was graduated from AAST He had several years of experience in marine engineering field.

Dr. **Mohamed Shehadeh** is currently Associate Professor at Marine Engineering Dept., Arab Academy for Science and Technology. He obtained BSc and MSc from Marine Engineering Dpt., AASTMT, Alexandria, Egypt and PhD from mechanical Engineering, Heriot Watt University, UK. He had participated in many European funds as well as works for seventeen years in design and research of mechanical and marine engineering fields.

Dr. **Ibrahim Hassan** is currently Associate Professor at Department of Basic and Applied Sciences, AASTMT, Alexandria, Egypt. He obtained BSc, MSc and PhD in Chemical Engineering, Faculty of Engineering, Alexandria University, Egypt. The author's major research interest is in the field of corrosion and mass-transfer processes. The author has a number of publications in this field. The author was a Post Doctoral Researcher during the period from February to September 2007and visitor professor during June to September 2010 and 2012 with The Chemical Engineering Department at Lakehead University, Thunder Bay, Canada.

Praise Worthy Prize

International Review of Chemical Engineering (I.RE.CH.E.), Vol. 6, N. 3
ISSN 2035-1755 *May 2014*

On the Initial Stage in Potato Immersion Frying

Luis T. Villa[1], Angélica C. Boucíguez[2], Ricardo F. Lozano[2]

Abstract – *In this paper, a descriptive mathematical model for the dynamical behavior of the free moisture desortion front inside of a potato sample, along the initial step (named also as vigorous bubbling stage) of an immersion frying process in oil heat is formulated and solved. Such model was generated using some information provided in an author's previous paper where, an initial free boundary value problem (IFBVP) was formulated as a mathematical model to describe the simultaneous heat and free moisture transfer during the stage of the process.*
Local in time, monotone dependence of the free moisture desorption front, upon a kinetic parameter in term of the oil bath temperature is also analyzed.

Keywords*: Potato Immersion Frying, Free Moisture Front, Initial Free Boundary Models*

Nomenclature

A	Lateral surface area (m^2)
C	Volumetric mass concentration (kg/m^3)
C_s	Heat capacity of solid (potato) in core region (J/kg °C)
C_0	Heat capacity of solid (potato) in crust region (J/kg °C)
D	Moisture diffusion coefficient (m^2/s)
d	Parameter defined by Eq. (20)
h	Convective heat transfer parameter (W/m^2 °C)
h_c	Enthalpy of potato in crust region (J/kg)
h_s	Enthalpy of potato in core region (J/kg)
H_v	Enthalpy of vapor (J/kg)
ΔH_v	Latent heat of vaporization (J/mol)
k_c	Effective thermal conductivity in crust region (W/m K)
k_s	Effective thermal conductivity in core region (W/m°C)
K_v	Hidraulic conductivity of the vapor (m^2)
l	Parameter defined by Eq. (20)
p_v	Vapor pressure (N/m^2)
Q	Function defined by Eq. (24)
R	Half – thickness of potato sample (m)
$S(t)$	Free boundary position at time t (m)
T	Temperature profile in the core region (°C)
u	Temperature profile in the crust region (°C)
T_b	Bulk temperature of oil bath (ºC)
Te	Vaporization temperature of pure water (ºC)
V_a	Specific molar volume of liquid water (m^3/kg)
V_v	Specific molar volume of vapor water (m^3/kg)
x,t	Spatial (m) and time (s) coordinate respectively

Greek letter

ε_a	Volume fractions of liquid water (m^3/m_t^3)
ε_v	Volume fractions of vapor water (m^3/m_t^3)
μ_v	Viscosity of the vapor (Pa s)
ρ_a	Density of water (kg/m^3)
ρ_v	Density of vapor water (kg/m^3)
ρ_c	Bulk density of solid (potato) in crust region (kg/m^3)
ρ_s	Bulk density of solid (potato) in core region (kg/m^3)

Subscripts

a	Water
b	Bulk
c	Regarding crust region
e	Ebullition
s	Regarding core region
t	Total
v	Vapor

I. Introduction

The immersion frying process of stick shaped natural potato in heat oil is a complex phenomenon. In fact, it involves simultaneous heat and mass transfer, chemical reactions, structural and textural changes, shrinkage or puffing, start gelatinization [1]-[5].

Farkas, *et al*. [1] provided a clear definition for such process. Just, such reference constitute a pioneer work on that study, in what regard the analytical predictive model formulation and solution for moisture concentration and temperature profiles inside the potato sample. Such as it can be seen in the pioneer work, the global process of immersion frying in oil heat applied to stick shaped natural potato, was consigned as occurring in several successive temporal steps: Preheating, Initial or vigorous bubbling and principal. Recently, in Villa *et al*. [2], a mathematical model in order to describe the initial step of the process which concern us, was formulated.

Manuscript received and revised April 2014, accepted May 2014

Such model consisted in an IFBVP associated to the free moisture concentration and temperature profiles.

For details on basic physic – chemical considerations, experimental evidence and other related information concerning the occurrence of the step, under analysis, we refer to the preceding cited work.

In Fig. 1 a schematic representation of a cross – section for a prismatic potato sample (length *L*, thickness 2*R*) along the evolution of the "Bubbling Stage" of the immersion frying is illustrated.

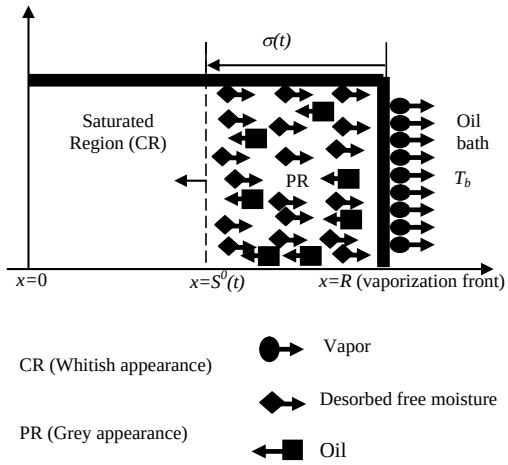

Fig. 1. Cross –section of potato sample with an orthogonal axial plane at *L*/2

Notice that the free moisture begin to be vaporized on the interfacial contact surface potato – oil heat, $x=R$; being R the half thickness of the sample measured from its geometrical center ($x=0$) and x the corresponding spatial coordinate ($0 \le x \le R$)

Hence, once that the "Bubbling Stage" starts, the free moisture desorption occur on the moving front localized at each time t ($t>t_1$), by the moving coordinate $x(t)= S^0(t)$ ($S^0(t_1)=R$, with t_1 the pre heating time for sample, that is the time in which the surface sample reach the water boiling point). Then the free boundary $x(t)= S^0(t)$ moves from the external surface $x=R$ to the center of the sample as the process progresses and divides the sample in two regions named Peripheral (PR) and Core Region (CR) respectively, such as it can be seen in Fig. 1.

The CR contain free moisture at saturation concentration; the PR contain desorbed free moisture diffusing toward the vaporization front $x=R$.

II. The Referential Model

In Villa *et al*.[2], in order to describe the initial step of an immersion frying process applied to stick shaped potato samples, such as it is schematized in Fig. 1, a mathematical model consisting in the following set of equations was reported:

$$\rho_s C_s \frac{\partial T}{\partial t} = k_s \frac{\partial^2 T}{\partial x^2} \qquad t > t_1 \qquad 0 < x < R \tag{1}$$

$$\frac{\partial T}{\partial x}(0,t) = 0 \qquad t > t_1 \tag{2}$$

$$k_s \frac{\partial T}{\partial x}(R,t) - \Delta H \cdot D \frac{\partial C}{\partial x}(R,t) = F \tag{3}$$

$$F = h\left[T_b - T(R,t)\right] \tag{4}$$

$$T(x,t_1) = Q(x) \qquad 0 \le x \le R \tag{5}$$

$$C(x,t) = C_0 \qquad t > t_1 \qquad 0 \le x \le S^0(t) \tag{6}$$

$$C(x,t_1) = C_0 \qquad 0 \le x \le R \tag{7}$$

$$\frac{\partial C}{\partial t} = D \frac{\partial^2 C}{\partial x^2} \qquad t > t_1 \qquad S^0(t) \le x \le R \tag{8}$$

$$C\left(S^0(t),t\right) = C_0 \qquad t > t_1 \tag{9}$$

$$-AD \frac{\partial C}{\partial x}(R,t) = \omega_v \qquad t > t_1 \tag{10}$$

$$\left(C^0 - C_0\right) \frac{dS^0}{dt} = -D \frac{\partial C}{\partial x}\left(S^0_+(t),t\right) \qquad t > t_1 \tag{11}$$

$$S^0(t_1) = R \tag{12}$$

The meaning of function, parameters, physical properties and data implied in (1) – (12) are provided in Nomenclature.

III. An Initial Value Problem to Describe the Dynamical Behavior of the Free Moisture Desorption Front

III.1. Basic Considerations

At this point, in order to take up a descriptive model formulation for the dynamical behavior of the free moisture desorption front $S^0= S^0(t)$, during the initial of the immersion frying process, which concern us, the following consideration is remarked:

(C1) taking into account basic physic – chemical knowledge on the process, it is known that along the Initial Step, the dynamical characteristics of the immersion frying is essentially governed by the free – moisture vaporization on the interfacial front potato – oil bath $x=R$.

In such step, the controlling phenomena is the free - moisture transfer for Fick diffusion trough PR, from the desorption front $x= S^0(t)$, being the free moisture vaporization a strong mass sink which means a driven force in the process.

III.2. Model Formulation

In view of the preceding consideration (C1), we will deduce a descriptive model in order to analyze the dynamical behavior of the desorption front $S^0 = S^0(t)$, working on the sub model consigned by equations (5) to (12). To begin with, we introduce the function $M=M(t)$, given as:

$$M(t) = 4L\left[R\int_{s^0(t)}^{R} C(x,t)\,dx + S^0(t)\int_{s^0(t)}^{R} C(x,t)\,dx \right] \quad (13)$$

Such function gives the amount of desorbed free – moisture on the desorption front $x = S^0(t)$, contained in PR ($S^0(t) \le x \le R$), at time $t>t_1$. On the other hand, from (13) it follows that:

$$\frac{dM}{dt} = 4L\frac{dS}{dt}\left[C_0\cdot\left(R+S(t)\right) - \int_{S(t)}^{R} C(x,t)\cdot dx \right] \quad (14)$$

and, from a mass balance applied to the desorbed free moisture contained in PR we have:

$$\frac{dM}{dt} = 4LD\left(R+S^0(t)\right)\frac{dC\left(S_+^0(t),t\right)}{dx} - AD\frac{dC(R,t)}{dx} \quad (15)$$

Now, we note that the mass conservation on the moving desortion front $x = S^0(t)$ provide the equation:

$$-D\frac{dC\left(S_+^0(t),t\right)}{dx} = \left(C^0 - C_0\right)\frac{dS^0}{dt} \quad (16)$$

This last equation play a role of Stefan condition in heat conduction with change phase on the free boundary.

Now, we shall use the following expression for the vaporization kinetic $\omega_\upsilon(t)$ in Eq. (9):

$$\omega_\upsilon(t) = 4R^2L\left(\rho_s + C^0\right)\frac{K_x}{60}\left(X_0 - X_e\right)exp\left(\frac{K_x t}{60}\right) \quad (17)$$

Such expression was reported in Krokida et al [3] concerning a potato immersion frying process under similar operative conditions which concern us.

In Krokida et al [3], empirical equations were postulated for K_x (kinetics vaporization coefficient) and X_e (moisture content at equilibrium) as functions of the media temperature of the oil bath, the cross sectional thickness of potato sample and percentage of hydrogenation concentration in oil heat. In (17), ρ_s and X_0 denote the mass density and the initial moisture content of the potato sample, respectively.

Then, taking into account Eqs. (5) – (12), and furthermore Eqs. (14) – (17), the following representation for the time derivative dS^0/dt is obtained:

$$\frac{dS^0}{dt} = \frac{-4R^2L\left(\rho_s + C^0\right)\frac{K_x}{60}\left(X_0 - X_e\right)exp\left(\frac{K_x t}{60}\right)}{8L\left[\left(C^0 - 2C_0\right)\left(R+S(t)\right) + \int_{S^0(t)}^{R} C(x,t)\,dx\right]} \quad (18)$$

More briefly, Eq. (19) can be written as:

$$\frac{dS^0}{dt} = \frac{-d\,exp(-bt)}{\ell\left(R+S(t)\right) + \int_{s^0(t)}^{R} C(x,t)\,dx} \quad (19)$$

where the parameters b, d and ℓ are defined by:

$$b = \frac{K_x}{60} \qquad d = \frac{a}{8L} \qquad \ell = \left(C^0 - 2C_0\right) \quad (20)$$

with a is given as:

$$a = 2R^2L\left(\rho_s + C^0\right)\frac{K_x}{60}\left(X_0 - X_e\right) \quad (21)$$

At this point, an idea reported as a specific contribution of the paper concerning the analysis trying to get light on the dynamical behavior of the free moisture desorption front in the initial step of a potato immersion frying process, is introduced. Such idea consist in to defined a new unknown function $v=v(t)$ as:

$$v(t) = \int_{s^0(t)}^{R} C(x,t)\,dx \quad (22)$$

Consequently, taking into account Eqs. (5) to (10), and (19), from (22), the following representation for the time derivative of function $v=v(t)$ is obtained:

$$\frac{dv}{dt} = \left[\frac{-1}{2R} + \frac{C^0}{\ell\left(R+S(t)\right)+v(t)}\right] d\,exp(-bt) \quad (23)$$

Hence, in view of (19), (22) and (23), the following Initial Value Problem (IVP) associated to two non – linear coupled first order differential equations is formulate:

$$\frac{dS^0}{dt} = \frac{-d\,exp(-bt)}{\ell\left(R+S^0(t)\right)+v(t)} \quad t > t_1 \quad (24)$$

$$\frac{dv}{dt} = \left[\frac{-1}{2R} + \frac{C^0}{\ell\left(R+S^0(t)\right)+v(t)}\right] d\,exp(-bt) \quad t > t_1 \quad (25)$$

$$S^0(t_1) = R \qquad v(t_1) = 0 \quad (26)$$

We note that, just the IVP (24) – (26) provide the announced descriptive mathematical model for the dynamical behavior of the free moisture desorption front $S^0 = S^0(t)$.

III.3. Model Solution

An efficient commercial version of soft *Mathematica*, was used to solve numerically (24) – (26), for the specific case of a prismatic potato sample with geometric dimension R=0.01m, and L=0.08m and the following values for parameters b, d, ℓ, and C^0:

$$X_0 = 3.34 \quad X_e = 0.84$$

$$b = 0.013 \quad d = 0.00155 \quad \ell = 435.6 \quad C^0 = 869.6 \quad (27)$$

$$\rho_s = 1050 \quad C_0 = 217$$

reported from bibliography concerned with potato physical data for Argentina variety commonly used to fast food. In particular, the kinetic coefficient b was reported from Krokida et al [3], when the oil bath temperature is 170 ºC. In Fig. 2 below, a graphical representation obtained using data corresponding to the numerical solution of (24) – (26) is illustrated. In the same figure, a comparison between the model solution for the free moisture desorption front $S^0(t)$ and experimental data can be observed. A good agreement is exhibited.

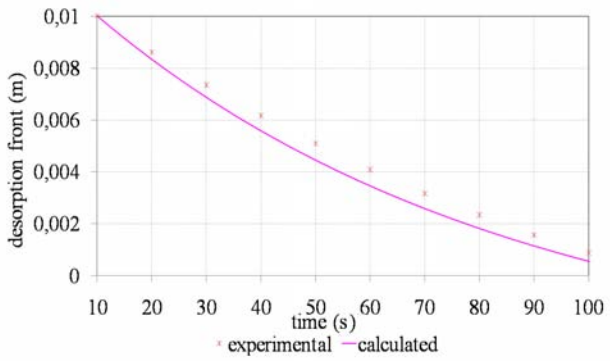

Fig. 2. The calculated desorption front S^0 as function of t and the comparison for the corresponding experimental results

IV. Influence of the Oil Bath Temperature on the Dynamical Behavior of Free Moisture Desorption Front

IV.1. A Local Result in Time

According to information reported in Krokida et al [3], the influence of the oil bath temperature play a role through the parameters b, a, and d, introduced by eqs. (20). Anyway, in view of the non-explicit dependence of the right hand side of Eqs. (24) – (26) upon such parameters, in what follows a parametric dependence analysis only deduced for a first order approximation to the solution of the IVP (24) – (26), will be reported.

We recall that, such parametric dependence result hold also for the solution $S^0(t)$ to (24) – (26), since the derivate of the such function at initial time $t=t_1$ is the same as the derivate of the function $S^0{}_1(t)$, given by eq. (30) below, which is the first order approximation of $S^0(t)$:

$$S^0(t) = R - d\int_{t_1}^{t} \frac{exp(-b\tau)}{\ell\left(S^0(\tau)+R\right)+v(\tau)}\,d\tau \qquad (28)$$

$$v(t) = \frac{-d}{2R} - C^0 d\int_{t_1}^{t} \frac{exp(-b\tau)}{\ell\left(S^0(\tau)+R\right)+v(\tau)}\,d\tau \qquad (29)$$

Hence, from (28) and (29), the following first order approximate solution for $S^0(t)$, is obtained:

$$S_1^0(t) = R - \frac{d}{2Rb\ell}\left[exp(-bt_1) - exp(-bt)\right] \qquad t > t_1 \quad (30)$$

It is important to observe that eqs. (28) and (29) constitute an equivalent integral representation of the differential model consigned by (24) - (26).

Adjusting information reported in Krokida *et al.* [3], to our case, the following empirical correlations for parameters b and d, in term of bath temperature T_b, will be used:

$$b = \frac{0.78}{60}\left(\frac{T_b}{170}\right)^{1.61} \qquad (31)$$

$$d = \frac{R^2}{4}\left(\rho_s + C^0\right)b\left[X_0 - 0.84\left(\frac{T_b}{170}\right)^{-3.63}\right] \qquad (32)$$

that is to say:

$$d = K\left(\frac{T_b}{170}\right)^{1.61}\left[X_0 - 0.84\left(\frac{T_b}{170}\right)^{-3.63}\right] \qquad (33)$$

with:

$$K = \frac{0.78}{60}\frac{R^2}{4}\left(\rho_s + C^0\right) > 0 \qquad (34)$$

being a common value X_0=3.9 kg/kgdb (for Argentine potato sample). In fact, taking into account eqs. (31) and (33), it follows that oil bath temperature T_b, is a process parameter that affect significantly the dynamical behavior of the free moisture desorption front during the initial step of potato immersion frying.

Such fact is a direct consequence of the vaporization kinetic $w_v(t)$, defined by Eq. (17), dependence upon the kinetic parameter b and the equilibrium value X_e, for

moisture loss. Such two parameters were correlationed in term of T_b, (Krokida et al [3]). Taking into account eqs. (31), (33), and (34), a brief analysis of the function $S_1^0(t)$, given by Eq. (30), upon the parameter T_b, let us to establish the following local in time results, which provides a monotone decreasing behavior upon T_b:

$$\frac{dS_1^0(t)}{dT_b} < 0 \quad \text{if} \quad t_1 < t < \frac{1}{b*} \tag{35}$$

where b^* is given as:

$$b* = 0.013\left(\frac{180}{170}\right)^{1.61} \tag{36}$$

Such monotone decreasing behavior of function $S_1^0(t)$, illustrate in Fig. 3, taking different levels for bath oil temperature T_b, from 170 to 180 ºC is presented.

We recall that in Fig. 3, the upper curve (T_b=170ºC) corresponds to the solution of the model, (24) - (26) represented in Fig. 2, before.

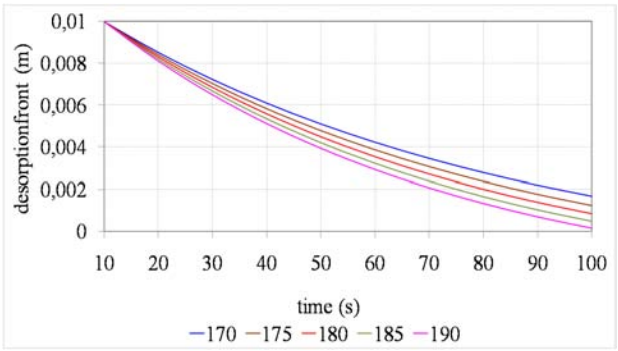

Fig. 3. Parametric dependence for desorption front upon the kinetic parameter *b*

V. Conclusion

Looking for to get light in what concern, the dynamical behavior of free moisture desorption front along the initial or vigorous bubbling step of potato immersion frying, a simple analytical descriptive model consisting in an Initial Value Problem (IVP) associated to two coupled nonlinear first order differential equations was formulated. For the usual case consisting in prismatic shaped potato sample, the numerical solution for the cited IVP was obtained as well as its comparison with experimental data. A good agreement is illustrated.

In order to obtain information concerning parametric influence on the dynamical behavior of the free moisture desorption front, an indirect strategy consisting in a pertinent analysis of a first order approximation to the solution of the descriptive model was developed. Such analysis reveled the oil bath temperature is a significant process parameter, in what regard the information searched. Here, it is remarked that an analysis concerning parametric influence of bath oil temperature in the original descriptive model (24) – (26) is a harder task.

Acknowledgements

This article was supported by Instituto de Investigaciones para la Industria Química (INIQUI) and Consejo Nacional de Investigaciones Científicas y Técnicas (CONICET) and Facultad de Ingeniería and Consejo de Investigaciones de la Universidad Nacional de Salta.

References

[1] Farkas, B.E.: Singh, R.P. & Rumsey, T.R. Modeling heat and mass transfer in immersion frying, part I: Model development. Part II: Model solution and verification. *Journal of Food Engineering*, 29, (1996) 211-226 and 29, 227-248 respectively.

[2] Luis T. Villa, Juan C. Gottifredi, Angélica C. Boucíguez, Some Considerations on a Simultaneous Heat and Mass Transfer Food Process. Model Formulation, (2011) *International Review of Chemical Engineering (IRECHE)*, 3 (2), pp. 265-271.

[3] Krokida, M.K. Oreopoulou, V. & Maroulis, Z. B. Water loss and oil uptake as a function of frying time. *Journal of Food Engineering* 44 (2000) 39-46.

[4] Michael Ngadi, Yunfeng Wang, Modeling Heat and Mass Transfer in Breaded Chicken Nuggets During Deep Fat Frying, (2009) *International Review of Chemical Engineering (IRECHE)*, 1. (6), pp. 506-514.

[5] Luis T. Villa, María C. Sanziel, Angélica C. Bouciguez, Numerical Solution and Validation Concerning a Descriptive Model of a Simultaneous Heat and Mass Transfer Process, (2011) *International Review of Chemical Engineering (IRECHE)*, 3 (4), pp. 493-498.

Authors' information

Luis Tadeo Villa Saravia. Born in Salta, Argentina, 25/05/45. Chemical Engineering, Universidad Nacional de Tucumán, Argentina, 1971. Science Doctor, Chemical Area. Universidad Nacional de Salta, Argentina, 2007. Teacher of high university level in applied mathematical area. His principal activity is the study of moving and free boundary problem in frying immersion process. Member of SIAM.

Angélica Carmen Boucíguez Born in Buenos. Aires, Argentina, 17/08/52. Degree in Physis. Universidad Nacional de la Plata, Argentina, 1978. Science Doctor, Renewable Energy Area. Universidad Nacional de Salta, Argentina, 2008. Teacher of high university level in Thermodynamics. Her principal activity is the study of moving and free boundary problem.

Ricardo Lozano: Born in Salta, Argentina, 22/04/60. Degree in Physis. Universidad Nacional de Salta, Argentina, 2011. Teacher of high university level in Thermodynamics. His principal activity is the study of moving and free boundary problem: modeling and numerical resolution.

Praise Worthy Prize

International Review of Chemical Engineering (I.RE.CH.E.), Vol. 6, N. 3
ISSN 2035-1755 *May 2014*

Performance Improvement of Adsorption Desalination Plant: Experimental Investigation

I. I. El-Sharkawy[1], K. Thu[1], K. C. Ng[1], B. B. Saha[2], A. Chakraborty[2], S. Koyama[2]

Abstract – *This article deals with the experimental investigation of a four-bed adsorption desalination (AD) plant working at a relatively high evaporation temperature. The effect of heat source temperature and adsorption/desorption cycle time on the system performance in terms of specific daily water production (SDWP) and performance ratio (PR) is experimentally studied. Owing to the higher evaporation temperature, SDWP of the plant is increased by two folds, to about 8.2 m^3 of water/ton-adsorbent per day. Further improvement is also achieved by using mass recovery scheme without significant changes to the AD plant.*

Keywords*: Adsorption, Desalination, Potable Water, Silica Gel-Water*

I. Introduction

With increasing world's population and the geographical mal-distribution of water resources, the scarcity of potable water is a serious problem that calls for practical solutions. The total amount of global water resources reserves is estimated to be about 1.4 billion cubic kilometres but fresh water constitutes only about 2.5% of the total reserves. Furthermore, the majority of fresh water in the world is trapped in the atmosphere, polar ice, underground and other inaccessible forms and only about 0.014% of the total fresh water is directly available to human activities [1], [2].

Desalination is a process by which the salinity in sea or brackish water, is removed and converted to potable or fresh water and it is a practical solution for solving the water shortage problems. Such processes can be divided into two groups. The first group is a heat-driven process (Distillation) such as multi-stage flashing (MSF), multiple effect distillation (MED) and solar distillation.

The second method employs electric power driven processes that include freezing, mechanical vapor compression, electro-dialysis and reverse osmosis [3]-[8].

All of the aforementioned types of desalination are found to be either highly energy-intensive or prone to serious corrosion and fouling problems when operated at elevated evaporating temperatures [9]. However, adsorption desalination (AD) plant differs in concept from the conventional desalination methods and the attractive features are as follows:

- It employs the low-temperature waste heat from industrial processes which are available in refineries, the co-generation plants, marine engines of ships and the power plants. The temperature waste heat needed to power the AD cycle are from 65˚ to 85˚C which is essentially "free" and if unused, and they would have been purged into the atmosphere.
- It is environmental-friendly as only silica gel ($SiO_2 \cdot nH_2O$) and water are employed as adsorbent-adsorbate pair.
- The AD cycle has almost no major moving parts except the valves for the vapor and coolant flows.
- It has low electricity usage as water pumps are used only.

The advantages of an AD cycle over other conventional methods would become apparent with the analysis of the specific energy consumption (kWh per m^3 of water).

Table I compares the energy cost of water production between the AD cycle and the conventional methods, such as the MSF, MED, and RO. In spite of the laboratory scale experiments, the AD cycle is found to give the lowest energy consumption at about 1.5 kWh per m^3 or equivalent to US$0.013 per m^3 whilst the highest cost of production is derived by the MSF at US$0.647.

With economy of scale of a full-scale plant, the energy consumption rate of AD method could be reduced to 1.2 kWh/m^3 as the parasitic pumping consumption is decreased. In this study, the performance of a four-bed adsorption desalination plant, in terms of the specific daily water production (SDWP) and performance ratio (PR), is experimentally investigated. The plant is operated at a relatively high evaporation temperature inside the evaporator where the cooling load is balanced by raising the chilled water inlet temperature to nearly that of the ambient. The effects of operating conditions such as the heat source temperatures, operation cycle time are discussed. Furthermore, the AD cycle employs the mass recovery scheme which further boosts the production of condensate.

II. Adsorption Desalination Plant

A pilot adsorption desalination (AD) plant has been

Manuscript received and revised April 2014, accepted May 2014

constructed and operated in the Air Conditioning Laboratory at National University of Singapore (NUS). Figs. 1(a) and 1(b) show the schematic diagram and a pictorial view of the four-bed adsorption desalination plant, respectively. The AD plant comprises six heat exchangers, namely four units of adsorption/desorption reactors or beds, the condenser and evaporator. The desalt operation of the AD cycle is similar to that of the four-bed adsorption chiller [11] and the detailed operation has reported recently by Wang and Ng [12].

The main difference between the operations of the AD and the chiller cycles lies in that saline solution is pre-treated before supplying to the evaporator and the condensate water that emanates from the condenser is removed as the pure water, using either a vacuum pump or a 10 m high liquid-filled U-tube. The overall system operation can be summarized as follows:

(i) The saline or brackish water is first pre-treated (e.g., filtering and de-aeration) and feeds to the evaporator. Purging of solution from the evaporator is conducted periodically for salt concentration control.
(ii) The sea water is dosed into the stainless steel evaporator where an external water circuit provides the heating load for maintaining the evaporator's temperature and pressure. Evaporation inside the evaporator is enhanced by using the spray water method instead of pool boiling technique.
(iii) The water level inside the evaporator is regulated for both the water level and concentration and this prevents the corrosion of the evaporating unit.
(iv) The evaporator is connected with the adsorbers where the evaporated water vapor is adsorbed by the silica gel. The heat of adsorption is removed by coolant from cooling tower during the adsorption cycle.
(v) The desorption-condensation process takes place at the condenser pressure where the desorbers are heated up to the desorption temperature with an external heat input. The desorbed vapor is condensed in the condenser where the heat of condensation is removed by the cooling water from the cooling tower.
(vi) The condensate is collected in a collection tank which is either intermittently pumped out to the ambient or extracted via a 10 m high U-tube.

III. Definitions and Modeling

The energy balance equations, the isotherm equation and the kinetic that are used for the evaluation of the performance of the adsorption desalination plant are presented below. Tóth isotherm equation can accurately provide the equilibrium amount of water vapors that the silica-gel can adsorb at specific temperature and pressure of the adsorbent, i.e.:

$$q^* = \frac{K_0 \exp\left(\Delta H_{ads} / RT\right) p}{\left[1+\left(K_0 / q_m \exp\left(\Delta H_{ads} / RT\right) p\right)^t\right]^{1/t}} \quad (1)$$

here q_m is the maximum adsorption amount, ΔH_{ads} is the enthalpy of adsorption, R is the gas constant, T is the adsorption temperature in Kelvin, K_0 and t are constants.

The adsorption kinetic can be expressed as follow:

$$\frac{dq}{dt} = \frac{15 D_{so} \exp\left(-E_a / RT\right)}{R_p^{\,2}}\left(q^* - q\right) \quad (2)$$

where D_{s0} is the pre-exponential constant, E_a is the activation energy, R_p is the particle radius and q denotes the instantaneous uptake. The heat of evaporation is calculated using the load water inlet and outlet water temperatures:

$$Q_{evap} = \dot{m}_{chilled}\, Cp_{(T_{EVAP})}\left(T_{chilled(in)} - T_{load(out)}\right) \quad (3)$$

The desorption heat and adsorption heat can be calculated using the temperatures of heating source and cooling for desorption and adsorption as follows:

$$Q_{des} = \dot{m}_{hot} Cp_{(T_{des})}\left(T_{hot(in)} - T_{hot(out)}\right) \quad (4)$$

$$Q_{ads} = \dot{m}_{cooling} Cp_{(T_{ads})}\left(T_{cooling(out)} - T_{cooling(in)}\right) \quad (5)$$

The following equation is used to calculate the amount of heat that is rejected at the condenser:

$$Q_{cond} = \dot{m}_{cond}\, Cp_{(T_{cond})}\left(T_{cond(out)} - T_{cond(in)}\right) \quad (6)$$

In the above mentioned equations, $\dot{m}_{hot}$, $\dot{m}_{cooling}$, $\dot{m}_{chilled}$ and $\dot{m}_{cond}$ are the mass flow rates of hot water, adsorber cooling water, chilled water, and condenser cooling water, respectively. $T_{hot(in)}$, $T_{cooling(in)}$, $T_{chilled(in)}$ and $T_{cond(in)}$ stand for a hot, cooling, chilled and condenser water inlet temperatures. $T_{hot(out)}$, $T_{cooling(out)}$, $T_{chilled(out)}$ and $T_{cond(in)}$ are hot, cooling ,chilled and condenser water outlet temperatures, respectively.

To evaluate the amount of water that can be produced by the AD cycle, the term specific daily water production is used and it can be calculated using the following equation:

$$SDWP = \int \frac{3600\, dQ_{cond}}{h_{fg(T_{cond})} m_{sg}} \tau\, dt \quad (7)$$

where τ is the number of running hours for the plant. For more accurate and realistic results, Q_{cond} is used to evaluate SDWP. However, in real calculation of the water production, the readings from the flow meter are used as follows:

$$SDWP = \frac{1440}{N} \frac{\sum_{i=1}^{N} (F)_i}{m_{sg}} \quad (8)$$

TABLE I
ENERGY COSTS COMPARISON FOR VARIOUS METHODS OF DESALINATION

Method of Desalination	Thermal energy consumed kWh/m^3 (A)	Electric energy kWh/m^3 consumed (B)	Primary fuel input k h/m^3 C= (A/ η_b+B/ η_c)	Energy cost of water US$ per m^3= $5*(C*3.6)/1055$
Multi-stage Flash (MSF)	19.4	5.2	37.9	0.647
Multi-effect Distillation (MED)	16.4	3.8	30.5	0.520
Vapour compression (VC)	-	11.1	29.2	0.497
Reverse Osmosis (RO) – single pass	-	8.2	21.5	0.366
Reverse Osmosis (RO) – double pass	-	9.0	23.7	0.403
Adsorption desalination (*high-grade* water)	Energy from waste heat	**1.5**** Author's data [10]	**3.94**	**0.013**

In Table I, all data is extracted from Seawater Desalination in California, California coastal commission Chapter 1-: Energy Use section, http://www.coastal.ca.gov/index.html [14]. The conversion units of 1 AF = 1345 m^3, 1 million BTU (1.055 GJ) of Natural gas costs US$5 (adopted from Singapore's natural gas prices in 2005). The electricity conversion efficiency, η_c, of power plants is 38% and the efficiency of boiler is 80%. ** The authors believe that the parasitic pumping energy could be further reduced (about 1.2 kWh/m^3) in a full scale plant where the pumping operation is much more efficient

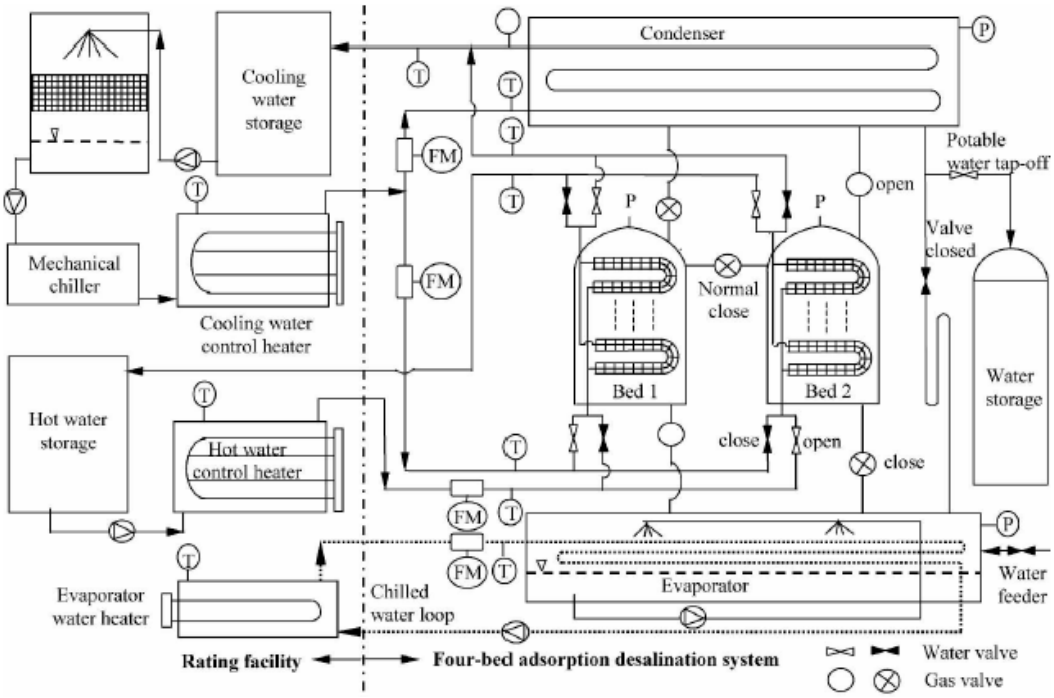

Fig. 1(a). Schematic diagram of a four-bed adsorption desalination plant in NUS

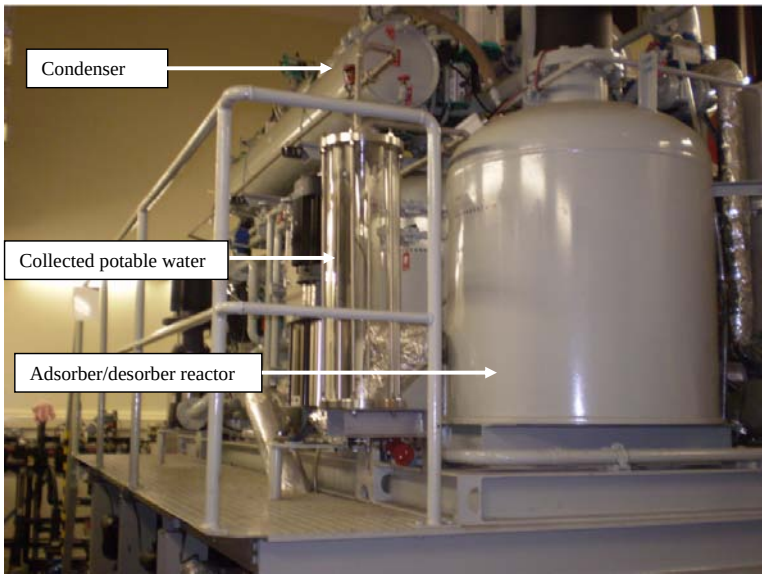

Fig. 1(b). Pictorial view of the a four-bed adsorption desalination plant (condenser side view)

In (8) F is condensate water flow rate measured in LPM and m_{sg} is mass of silica-gel used. The performance ratio of the adsorption desalination process is expressed as follow:

$$PR = \int \frac{\dot{m}_{water} h_{fg(Tcond)}}{dQ_{des}} dt \quad (9)$$

IV. Mass Recovery Scheme

A practical and yet simple scheme that has been demonstrated in the prototype of a four-bed adsorption desalination plant is the mass recovery by using a pressure equalization (PE) technique [13]. The principles of pressure equalization is best understood by using the *P-T-q* diagram (see Fig. 2).

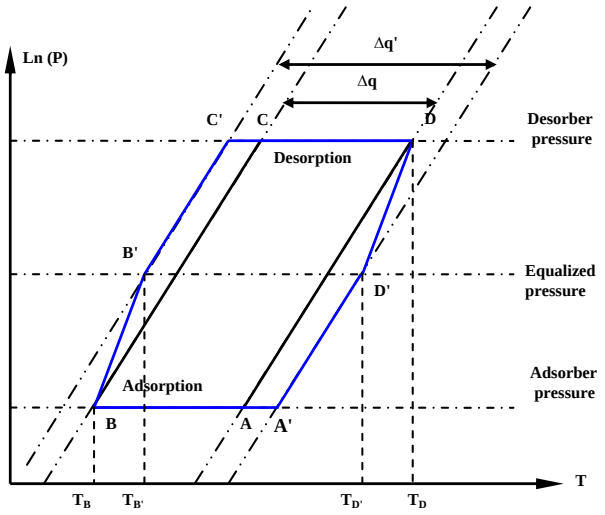

Fig. 2. Dühring Diagram showing the pressure equalization process

As can be seen from Fig. 2, at the end of adsorption/desorption processes, the pressure of the desorber reactor is nearly equal to that of the condenser and the refrigerant (water) concentration reaches its minimum value (q_D), which is the saturation state corresponding to the desorption temperature and condenser pressure.

On the other hand, the pressure of adsorber is controlled by that of the evaporator and the concentration reaches it the saturated state (q_A), corresponding to the adsorber reactor pressure and the adsorption temperature.

By connecting both of the adsorber and desorber reactors for a short time at the end of adsorption/desorption processes, refrigerant vapor in the desorber is forced to move to the adsorber by pressure swing action making the silica gel dryer and the refrigerant uptake decreases to $q_{D'}$. The simulations pressurization in the adsorber causes silica gel state to adsorb more refrigerant, and the uptake reaches to $q_{B'}$.

Mass of refrigerant circulated in the system is then increased to ($q_{B'} - q_{D'}$) and thus improving the SDWP.

V. Results and Discussion

At a constant adsorption temperature, the adsorption capacity of silica gel - water pair increases with the increase of adsorption pressure. Therefore, SDWP can be significantly increased with the increase of the evaporation temperature of the evaporator. Evaporator pressure can be increased by increasing the chilled water inlet temperature.

It is noted that the SDWP can also be increased by using: (i) The recovery of heat by cooling the cooling water supplied to the adsorption process using a plate heat exchanger [10] and (ii) the tapping of heat to the evaporator by injecting part of the flow from cooling tower circuit. In the former method, the advantage lies in the cooling of silica gel during the adsorption process only to a temperature lower than ambient and thus enhancing the adsorption process of silica gel. The latter method lowers the supply temperature of coolant from the cooling tower, benefiting both the adsorber and condenser. Fig. 3 shows the improvements in SDWP and PR with the rage of operation time at the rated operation condition shown in Table II. The chilled water inlet temperature to the evaporator is kept constant at 30˚C. Experimental data show that the SDWP of the plant is increased by two folds, to about 8.2 m^3 of water/ton of adsorbent per day. Fig. 4 shows the effect of the hot water inlet temperature on the cycle SDWP and PR using a half-cycle time of 360s. It is noted that the SDWP increases linearly with increasing hot water inlet temperatures.

The improvement is attributed to the increased in vapor flow within the AD cycle at higher driving source temperatures. However, the increase in PR is only marginal. The increase in SDWP occurs due to the larger temperature difference between heat source and heat sink.

Fig. 5 shows effects of chilled water inlet temperatures on the cycle performance with and without heat exchange between the chilled water coming out from the evaporator and the cooling water supplied to the adsorber. Experimental results show that the SDWP increases linearly with the increase of chilled water inlet temperature. Due to the limitation of the used heat exchanger capacity the improvement in the SDWP is slightly low.

Fig. 6 shows the performance of adsorption desalination plant at different pressure-equalization (PE) time intervals, namely 10, 20 and 30 s. It can be seen that the SDWP increase by as much as 10 m^3 of water/ ton of adsorbent per day at a PE of 10s. However, an increase in the PE time beyond the optimal value reduces the SDWP due to the decrease of the mass transfer rates.

TABLE II
RATED APPLICATION CONDITIONS

	Temperature (°C)	Flow rate (LPM)
Hot water inlet (desorber)	85	48
Cooling water inlet (adsorber)	29.5	48
Cooling water inlet (condenser)	30	120
Mass of silica gel per bed (kg)	36	
Switching time (s)	40	

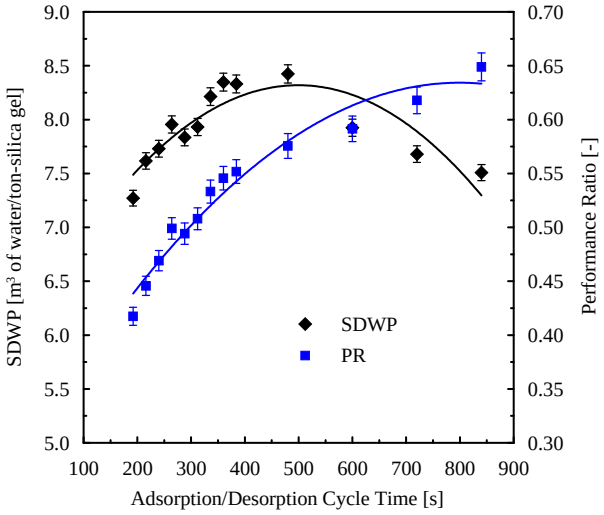

Fig. 3. Performance of the four-bed adsorption desalination system

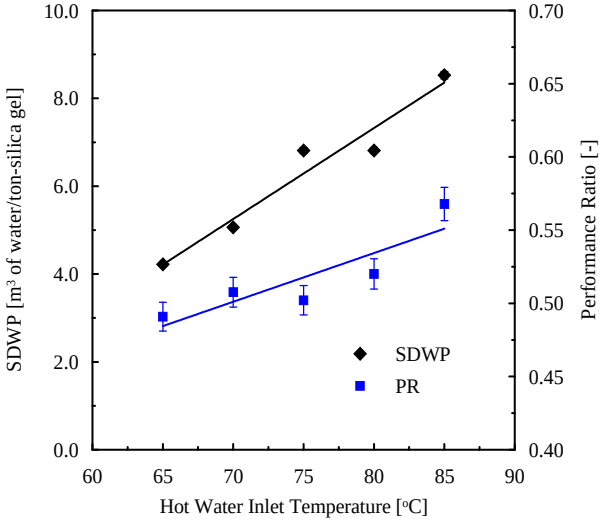

Fig. 4. Effects of the hot water inlet temperatures on the system performance

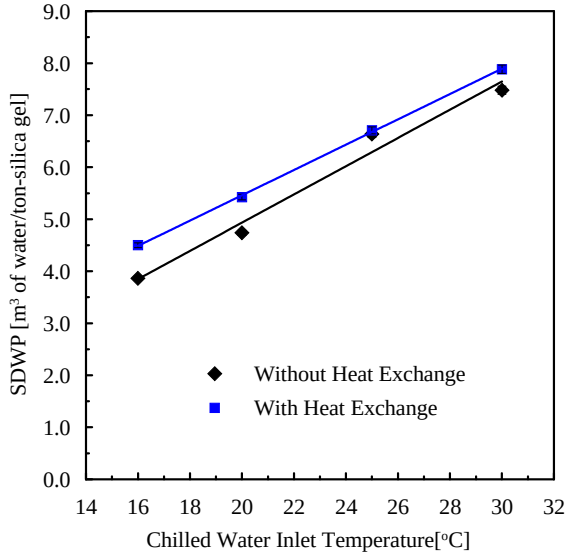

Fig. 5. Effects of the chilled water inlet temperatures on the system performance

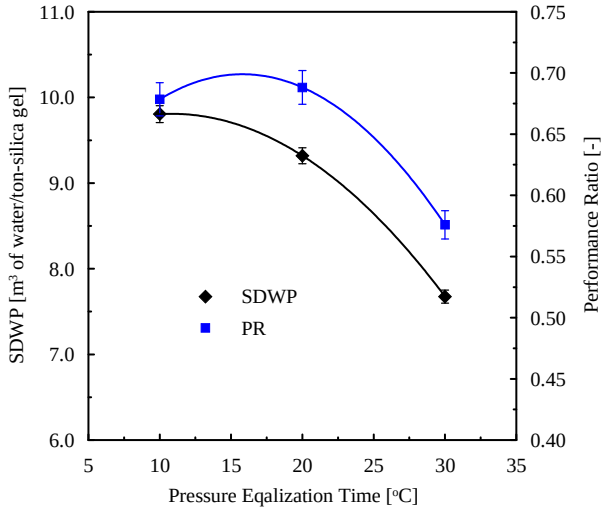

Fig. 6. Performance of 4-bed adsorption desalination plant with different PE times

VI. Conclusion

The performance a four-bed adsorption desalination plant has been experimentally investigated at chilled water inlet temperatures set near to the ambient temperature. Experimental results show that the plant produces daily potable water as much as 8.2 m^3 of water per ton of silica gel at inlet chilled water temperature of 30˚C. Further improvement in SDWP is achieved by employing a heat exchanger between the cooling water and the chilled water, and it has found that the SDWP could improve by about 22% at an optimal pressure equalization time of 10 s. The authors believe that further improvements of the system performance can be achieved by employing a more advanced heat and mass recovery schemes that would be easy adapted by AD cycle.

References

[1] S. Al-kharabsheh, D.Y. Goswami, Theoretical analysis of a water desalination system using low grade solar heat, *Journal of solar energy engineering transactions of the ASME* , Vol. 126, (2), pp. 774–780, 2004.

[2] Robert F. Service et al., Desalination Freshens up, *Science*, 313, 1088 , 2006.

[3] Y. Al-Wazzan, F. Al-Modaf, Seawater desalination in Kuwait using multistage flash evaporation technology- historical overview, *Desalination*, Vol. 134, pp. 257–267, 2001.

[4] M. Al-Shammiri, M. Safar, Multi-effect distillation plants: state of the art, *Desalination*, Vol. 126, pp. 45–59, 1999.

[5] H. Mosry, D. Larger and K. Genther, A new multiple–effect distiller system with compact heat exchangers, *Desalination*, Vol. 96, pp. 59-70, 1994.

[6] Z. Amjad, Reverse Osmosis: Membrane Technology, Water Chemistry, and Industrial Applications, Chapman & Hall, International Thomson Publishing (New York, 1993).

[7] Bart Van der Bruggen, Carlo Vandecasteele, Distillation vs. membrane filtration: Overview of process evolutions in seawater desalination, *Desalination*, Vol. 143, pp. 207-218, 2002.

[8] R.L. Hummel, Solar distillation with economies of scale, innovation and optimization, *Desalination*, Vol. 134, pp. 159-171, 2001.

[9] G. Ehrenman, From sea to sink, *Mechanical Engineering*, Vol. 126, 10, pp. 38–43, 2004.

[10] K.C. Ng, X.L. Wang, L.Z. Gao, A. Charkarborty, B.B. Saha, S. Koyama, A. Akisawa and T. Kashiwagi, Apparatus and method for desalination, *Singapore Patent Application no: 200503029-1*, 12th May ,2005.
[11] K.C. Ng, H.T. Chua, X.L. Wang, T. Kashiwagi, B.B. Saha, Prototype testing of a novel four-bed regenerative silica gel–water adsorption chiller, *ICR 0042, Washington DC, USA, 2003.*
[12] X.L. Wang and K.C. Ng, Experimental investigation of an adsorption desalination plant using low-temperature waste heat, *Applied Thermal Engineering*, Vol. 25, pp. 2780-2789, 2005.
[13] K.C. Ng, X. Wang, Y.S. Lim, B.B. Saha, A. Chakarborty, S. Koyama, A. Akisawa and T. Kashiwagi, Experimental study on performance improvement of a four-bed adsorption chiller by using heat and mass recovery, *International Journal of Heat and Mass Transfer*, Vol. 49, 19-20, pp. 3343-3348, 2006.
[14] Seawater Desalination in California, California coastal commission Chapter 1: Energy Use section, http://www.coastal.ca.gov/index.html - date of access is 15/01/2007.

Authors' information

[1]Department of Mechanical Engineering, 10 Kent Ridge Crescent, Singapore 119260.

[2]Interdisciplinary Graduate School of Engineering Sciences, Kyushu University, Kasuga-koen 6-1, Kasuga-city, Japan.

Ibrahim I. El-Sharkawy received his B.Sc. (Hons.) and M.Sc. degrees in Mechanical Engineering from Mansoura University, Egypt. He obtained his Ph.D. from Kyushu University, Japan in 2006. He is a faculty member at Mansoura University. Currently, he is joining Mechanical Engineering Department, National University of Singapore as a postdoctoral research fellow. His main research interests are thermally powered adsorption cooling systems and heat and mass transfer analysis. He has published more than 20 articles in peer reviewed journals and proceedings. He has won three conferences paper awards in 2004, 2005 and 2006, respectively.

Kyaw Thu received his Bachelor degree in Mechanical Engineering from Yangon Technological University (Y.T.U.), Myanmar, in 2004. Currently, he is a Ph.D. candidate at Mechanical Engineering department, National University of Singapore. His research area is adsorption desalination; experiments and simulation and thermally driven adsorption systems.

Professor Ng obtained his BSc. (Hons.) in Mechanical Engineering and PhD. from University of Strathclyde, Glasgow, United Kingdom, in 1975 and 1980, respectively. Prior to joining the NUS in 1981, he worked as a project engineer at the research center of Babcock Power (Glasgow, UK) where he was first introduced to many heat transfer problems in large boiler systems. He is now a tenured full professor in the Mechanical Engineering Department of the National University of Singapore, and is also a registered Professional Engineer (Singapore), a Chartered Engineer of the IMechE (UK) and a member of the Institution of Engineers, Singapore. His research interests include (a) modeling and testing of chillers, heat pumps and heat transformers, (b) solar collector testing and design, (c) waste heat recovery plants for district cooling and adsorption desalination. He has published more than 90 international peer-reviewed journals in topics related to his research, a similar number of international conference papers, and 6 patents to his credit. Recently, he has been awarded the Ludwig Mond Prize (2006) from the Process Division of the IMechE, UK.
E-mail: mpengkc@nus.edu.sg

Bidyut Baran Saha obtained his B.Sc. (Hons.) and M.Sc. degrees from Dhaka University, Bangladesh in 1987 and 1990, respectively. He received his Ph.D. in Mechanical Engineering from the Tokyo University of Agriculture and Technology, Japan in 1997. He is currently working as an Associate Professor at the Department of Energy and Environmental Engineering, Interdisciplinary Graduate School of Engineering Sciences, Kyushu University, Japan. His main research interests are thermally powered sorption systems, heat and mass transfer analysis and energy efficiency assessment. He has published more than 100 articles in peer reviewed journals and proceedings. He has edited two books and holds five patents.

Anutosh Chakraborty received his B.Sc. Eng. from BUET, Bangladesh in 1997. He obtained his M.Eng and Ph.D. degrees from the National University of Singapore (NUS) in 2001 and 2005, respectively. At present, he is working as a JSPS Fellow at Interdisciplinary Graduate School of Engineering Sciences, Kyushu University, Japan. His areas of research are micro/nano scale transport phenomena and energy conversion, thin film thermoelectric cooling/heating, adsorption science, and micro-electronics cooling. To date, he has published 20 peer-reviewed journal articles and 4 patents.

Shigeru Koyama is a Professor at the Department of Energy and Environmental Engineering, Interdisciplinary Graduate School of Engineering Sciences, Kyushu University, Japan. He is now the Vice President of Commission B1 of International Institute of Refrigeration (IIR). He received his Ph.D. in 1980 from Kyushu University, Japan. His main research interests are vapor compression systems, sorption systems, compact heat exchanger design, and heat and mass transfer analysis. He has published more than 190 articles in well-recognized journals, books and proceedings. He is an editor of the *Thermal Science and Engineering, Japan*.

Praise Worthy Prize

International Review of Chemical Engineering (I.RE.CH.E.), Vol. 6, N. 3
ISSN 2035-1755 *May 2014*

The Influence of Hydrogen and Chromium on Behavior Mechanic of the Welded Joints

A. Aboura[1], A. Seddak[2], A. Hebbar[3]

Abstract – *In this present work the effect of hydrogen on the mechanical behavior of the welded joint of two types of steels A42E26 and Z2CN18-10 was studied. The specimens of the tension test were manufactured in accordance with standard ASTM by machining from plane sheet. Hydrogen was superficially introduced at 50°C by the electrolytic method by using a solution acid $1NH_2SO_4$ with 0.25 g/l As_2O_3, a platinum anode and a density of current of 100 mA/cm^2 for various durations. The mechanical tests were carried out at ambient temperature and in air. With an aim of bringing a reflex ion on the influence of hydrogen and chromium on the mechanical behavior of the welded joints of two types of steels the A42E26 and Z2CN18-10, the experiments were carried out, by simultaneously varying parameters considered to be influential, to lead to the modeling of the maximum loading and Ultimate elongation.*

Keywords: *Stainless Steel, Welded Joint, Hydrogen Embrittelment, Design of Experiment*

I. Introduction

Steels are largely used in the industry of energy production, in particular the austenitic stainless steels, because of their good resistance to the phenomenon of the embrittelment by hydrogen (E.H). However several carried out work [1]-[4] shows a degradation of the ductility of the latter, which is often allotted at hydrogen interaction materials.

Hydrogen can dissolve in its materials and to modify their mechanical characteristics, this phenomenon causes much damage. The role of the structure is complex; however, the influence of hydrogen on the mechanical properties of the welded joints is more complicated.

The weld joints have a very significant influence. On the same specimen, the zones with coarse grains take care less than the zones with small grains [5].

The welded joint is heterogeneous as well its metallographic structure, its chemical composition, the constraints, as well as hydrogen.

The properties of the welded joints undergo the specific modifications, as well under the action of the hydrogen introduced into metal by the process of welding as under the action of the hydrogen which penetrates there after welding [6], [7].

By the application of the statistical methods of the experimental designs [8]-[11], one carried out experiments on joints welded in charge in hydrogen of two types of different materials and two methods of different welding one the arc manual and the other the TIG, by simultaneously varying parameters considered to be influential with an aim of modeling the maximum loading (Rm) and Ultimate elongation (A%).

II. Experimentation

II.1. Materials

The materials used in our experiment are the steel of type A42E26 and the stainless steel austenitic Z2CN18-10 whose chemical composition and the mechanical characteristics are given respectively to Tables I and II.

TABLE I
CHEMICAL COMPOSITION OF MATERIALS USED

Material (% w)	A42E26	Z2CN18-10
C	0.3	0.02
Mn	0.65	2
S	0.025	0.03
P	0.025	0.045
Si	0.10	1
V	0.08	-
Cr	0.4	18
Mo	0.15	-
Ni		10

TABLE II
MECHANICAL CHARACTERISTICS OF MATERIALS USED

Material	A42E26	Z2CN18-10
Rm [Mpa]	420	485
Re [MPa]	240	170
A [%]	30	<30
HB	163	<200

The specimens were adjusted by leaving spacing for the penetration of the filler. For the welding of the two types of steel, two operational methods were used to know:

- Welding the arc with electrode coated with a filler E7018 for steel A42E26 and a filler ER316L for stainless steel Z2CN18-10.

Manuscript received and revised April 2014, accepted May 2014

TABLE III
CHEMICAL COMPOSITION OF THE FILLERS MATERIALS

Elements (% weight)	E7018 (electrode coated)	ER70S4 (TIG-Filler)	ER316L (electrode coated)	ER316L (TIG-Filler)
C	0.06	0.1	≤0.03	≤0.03
Si	0.5	0.8	0.4	0.4
Mn	1	1.2	1.7	1.7
S	0.01	≤0.03	≤0.03	≤0.03
P	0.01	≤0.03	≤0.03	≤0.03
Cr	-	≤0.15	19	19
Ni	-	0.15	12.5	12.5
Ca	-	≤0.1	-	-
Mo	-	-	2.5	2.5

TABLE IV
MECHANICAL CHARACTERISTICS OF THE FILLERS MATERIALS

Mechanical Characteristics	E7018	ER70S4	ER316L
Re [Mpa]	465	440	425
Rm [Mpa]	545	540	590
A [%]	28	25	40
Z [%]	70	-	-
HB	180	-	-
Kcv [J/cm^2]		≥80 (-20°C) ≥50 (+40°C)	135 (+20°C)

TABLE V
EXPERIMENTATION OF THE TYPE $2^2.3^1$

Basic value	x_{i0}	11		300
Interval	Δx_i	07		300
Maximal Value	x_i	18	TIG	600
Minimal Value	x_{i0}	04	Arc	00

Unit		%		min	Interactions					R_m [MPa]	A [%]
N° of experiment		X_1	X_2	X_3	X_1X_2	X_1X_3	X_2X_3	$X_1X_2X_3$	X_3^2- 2/3	$\bar{Y}$	$\bar{Z}$
1		-	-	-	+	+	+	-	1/3	473.3	39.43
2		+	-	-	-	-	+	+	1/3	543.6	50.34
3		-	+	-	-	+	-	+	1/3	545.3	36.5
4		+	+	-	+	-	-	-	1/3	530	44.06
5		-	-	+	+	-	-	+	1/3	365.6	27
6		+	-	+	-	+	-	-	1/3	361.6	43
7		-	+	+	-	-	+	-	1/3	310	27.21
8		+	+	+	+	+	+	+	1/3	420	41.62
9		-	-	0	+	0	0	0	-2/3	438.2	33.78
10		+	-	0	-	0	0	0	-2/3	539.4	46.53
11		-	+	0	-	0	0	0	-2/3	448	34.06
12		+	+	0	+	0	0	0	-2/3	530	43.37

- Welding with process TIG with a filler ER 70S4 for carbon steel A42E26 and a filler ER316L for stainless steel Z2CN18-10 in wire.

The chemical composition and the mechanical characteristics of the fillers are given to Tables III and IV.

The chemical composition of the molten zone was determinate by using dilution (30%), knowing that it varies appreciably with the process of welding.

The contribution of base metals A and B is 15% that of the filler is 70%. Hardness is measured in the molten zone and the thermically affected zone, the operation is done in clean surfaces and smooth, applied to a rigid support with spacing from 3 to 4 mm between the prints.

II.2. Experimentation Procedure

The specimens, before being used in the stage of the mechanical tests, are polished with carbide paper of silicon until the n° 4000 and completion with felt soaked with slice colloidal in suspension, standard OPSOT.

The goal of this treatment makes it possible to remove oxide film formed during the former stage and which prevents the diffusion of hydrogen towards the interior of the material [12]. After polishing, the specimens are charged in hydrogen by the electrolytic method at 50°C by using an aqueous solution of sulphuric acid $1NH_2SO_4$ with $0.25g/l$ As_2O_3 [2].

The oxide is regarded as poison against the recombination of hydrogen in molecule [13]. The loading is under galvanic control which requires that two electrodes, the anode is in platinum; the specimen to charge is placed at the cathode [14]. The duration of the load varies from 1 at 8 hours with a density of current equalizes $100mA/cm^2$. The specimens after the loading are used in the following stage of the mechanical tests.

By the application of the statistical methods of the experimental designs, one carried out the mechanical tests, by using an experimental design of the type $2^2.3^1$ (Table V). The influential parameters are the chromium rate (X_1) which vary on two levels (-, +), the type of welding (X_2) on two levels (-, +), and the duration of

loading in hydrogen (X_3) which varies on three levels (-, 0, +).

III. Results and Interpretations

III.1. Maximum Resistance [Rm]

The criterion of Cochrane is equal to G = 0.135, the lower than *Gt* = 0.3924, dispersions is thus homogeneous. The confidence interval of the coefficients $\Delta\beta_i = t_{\alpha\ fy}$; for α =0.05 ; f_1= *N* (m-1) = 24 is equal to 1.52, with *t* (0.05, 24) = 1.71. In order to have a precision of the models, the coefficients of regression are given 4 digits after the comma. We consider only the significant coefficients of regression [$\beta_i \geq \Delta\beta_i = \pm t_{\alpha\ fy}$. $S(\beta_i)$], the model takes the form:

$$Y(X_i, \beta_i) = 39.845 + 2.868X_1 - 7.937X_3 + \\ +2.49\ X_1X_2X_3 - 4.52X_3^2 \quad (1)$$

The experimental value of the criterion of Fischer [8] is F_{exp} = 2.25. The model is adequate. For an average percentage out of chromium equal to 11%, the model will have the following form:

$$Y(X_i, \beta_i) = 39.845 - 7.937X_3 - 4.52X_3^2 \quad (2)$$

Its surface of answer is in the form of Fig. 1.

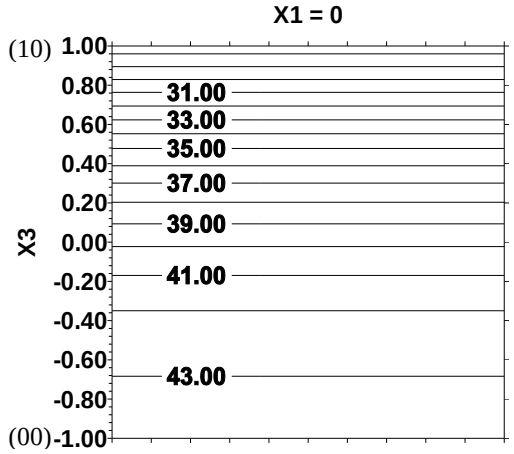

Fig. 1. Influence duration of loading on resistance maximum

Maximum resistance decrease linearly with the increase in the duration of loading in hydrogen. For an intermediate value between the two types of welding, the model will have the form:

$$Y(X_i, \beta_i) = 39.845 + 2.868X_1 + \\ -7.937X_3 - 4.52X_3^2 \quad (3)$$

Its chart is in the form of Fig. 2.

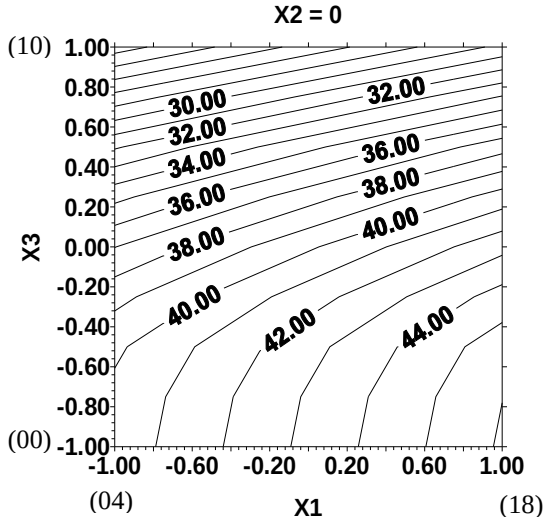

Fig. 2. Influence of chromium and duration of loading on the maximal resistance

The graph of Fig. 2 shows that the decrease of chromium in materials and the growth of the duration of loading in hydrogen from zero to four hours, weaken maximum resistance not linearly and slowly, where chromium has more influence than the duration of loading and from four to ten hours linearly and quickly and there the influence is reversed.

For an average value of the duration of loading in hydrogen (05 hours), the model will be:

$$Y(X_i, \beta_i) = 39.845 + 2.868X_1 \quad (4)$$

Its surface of answer (Fig. 3) shows that chromium is the only influential parameter on the maximum loading.

The increase in chromium in material lets linearly grow the load.

III.2. Elongation A [%]

By considering only the significant coefficients, the mathematical model will have the form:

$$Y(X_i, \beta_i) = 39.44 + 5.91X_1 - 3.94X_3 \quad (5)$$

The criterion of Fischer F_{exp} is equal to 0.20; the model describes elongation adequately. Its surface of answer will have the form of Fig. 4. Contours of Fig. 4 shows that by increasing the percentage of chromium in material, while decreasing the duration of loading in hydrogen, the elongation of material grows linearly.

IV. Conclusion

The influence of hydrogen on the mechanical properties of the welded joint is dependent with the distribution of hydrogen in the zone of the weld bead and the base metal. It is noticed that hydrogen decreases the

resistance and the plasticity of steels.

According to results' obtained, the influence of hydrogen is more significant in carbon steel than in the austenitic stainless steel. During welding, there is diffusion of carbon between the weld bead and the base metal. Generally, the diffusion is carried out base metal towards the weld bead, and consequently hydrogen has more chance to be better diffused in the base metal and it can occupy the sites released by carbon on the one hand and on the other hand the imperfections crystalline (gaps, dislocations, etc...), thus the capacity for absorption of hydrogen is more significant. In the austenitic stainless steel, austenite does not undergo a transformation; on the other hand, there is enlargement of the grain, under the effect of the high temperature, in the weld bead. Contrary to the case of carbon steel, hydrogen occupies the existing defects in the austenitic stainless steel with a weak absorption.

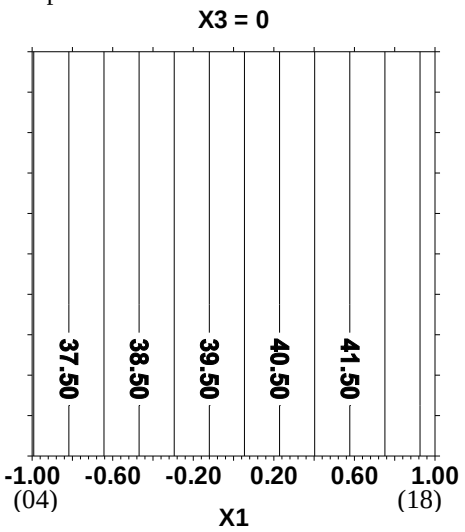

Fig. 3. Influence of chromium on the maximal resistance

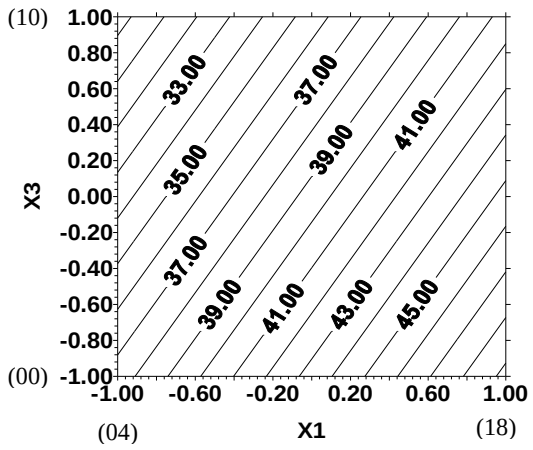

Fig. 4. Influence of chromium and duration of loading on the elongation

References

[1] L.W. Tsay, M.C. Young, C. Chen, Fatigue crack growth behaviour of laser-processed 304 Stainless steel in air and gaseous hydrogen, (Corrosion Science,V.45, pp. 1985-1997, 2003).

[2] A. M. Brass, Jacques Chêne, Lionel Coudreuse, Fragilisation des aciers par hydrogène, Étude et prévention, (Tech.Ing.MB2 pp. M175.1-24; M176.1-12, 2002).

[3] T. J. Carter, L. A. Cornish, Hydrogen in Metal, (Engineering Failure Analysis, pp. 113-121, 2001).

[4] J. H. Huang, Internal hydrogen induced subcritical crack growth in austenitic stainless Steel, (Metallurgical Transaction A, V.22A, pp. 2605-2618, 1991).

[5] D. Desjardin, RLTR, Corrosion sous contraintes phénomène et mécanisme. (Bonbonnes, 1990).

[6] A. Leroy, (Soudage et techniques connexes, pp. 375-383, 1983).

[7] C. Pan and Col., Hydrogen embrittelmente of weld metal of austenitic stainless steels, (Corrosion Science, pp. 1983-1993, 2002**).**

[8] H. Bandemer., A. Bellmann, Statistische Versuchs plannung, (Teubner Verlag, Leipzig, 1976).

[9] S. Vivier, Stratégie d'optimisation par la méthode des plans d'expériences et application aux dispositifs électroniques modélisés par éléments finis, (Thèse de Doctorat, Ecole centrale de Lille, 2002).

[10] F. Gillon, Modélisation et optimisation par les plans d'expériences d'un moteur à commutations électroniques, (Thèse de Doctorat, Ecole centrale de Lille, 1997).

[11] E. Scheffler, Einfürung in die Praxis der statistischen Versuchsplannung, (VEB þdeutscher Verlag für Grundstoffindustrie, Leipzig, 1986).

[12] K. Shimizu, H. P. Habazaki, G. E. Thompson and G. C. Wood, GDOES depth profiling analysis of the air-formed oxide film on a sputter-deposited Type 304 stainless steel Surf., (Interface Anal. 29, pp.743-746, 2000).

[13] N. K. Kuromoto, A. S. Guimaraes, C. M. Lepiendki, Materials Sciences and Engineering, (A381, pp. 216-22, 2004).

[14] T. P. Perng, J.K. Wu, A brief review note on mechanisms of hydrogen entry into metals, (Materials Letters 57, pp. 3437-3438, 2003)

[15] N. Narita, H.K. Birnbaum, On the role of phase transitions in the hydrogen embrittlement of stainless steels, (Scripta Metall, pp. 1355-1358, 1980).

[16] A. J. McEvily, I. LeMay, Hydrogen-Assisted Cracking, (Materials Characterization 26, pp.253-268, 1991)

Authors' information

[1]Lecturer investigator, Department of Mechanic, University of Mostaganem, Algeria, B.P. 1156 – R.P – 27000 Mostaganem, Algeria.
E-mail: a_aboura@hotmail.com

[2]Lecturer, Department of Mechanic, University of Technology, Oran, Algeria.

[3]Lecturer, Department of Mechanic, University of Mostaganem, Algeria, B.P. 882 – R.P – 27000, Mostaganem, Algeria.

Ahmed Aboura born at the 10/08/1957 in Chlef , Algeria, Master degree in materials, Lecturer investigator in the department of mechanics, University of Mostaganem, Algeria. Ahmed has conferences in hydrogen and currently deals with the wear of materials. Ms. Aboura is member of the scientific council of mechanical department.

International Review of Chemical Engineering (I.RE.CH.E.), Vol. 6, N. 3
ISSN 2035-1755 May 2014

Concentration Dependency of the Rheological Behaviour of Oil-Water Emulsions

L. Benali

Abstract – *The evolution of viscosity with the oil concentration was measured in a rotating cylinder viscosimeter. The measurements were performed for an oil emulsion used for lubrication of drilling and cutting tools and for crude oil emulsions. At low concentrations the rheological behaviour of the lubricant emulsion is weakly Binghamian. At higher concentrations a power law model was used to fit the data. For both emulsions a peak of viscosity was observed for an concentration ranging between 70 and 80 vol%. The results have also show that a Richardson like exponential model of the viscosity evolution with concentration is only valid for high shear rates and concentrations close to the critical concentration corresponding to the peak of viscosity.*

Keywords: *Concentration, Crude Oil Emulsion, Cutting Oil Emulsion, Peak of Viscosité, Rheological Behavior*

I. Introduction

Knowledge of emulsions rheological behaviour is of major importance for industrial applications. After its development in traditional domains like chemical or cosmetic industry, emulsion technology has found a renewed success with applications in different domains as food or oil industry.

For the first, increase of production of industrially prepared foods has brought to a systematic use of emulsifiers. The final aspect of the product, generally directly related to its rheological behaviour, is of major importance for the consumer. On the other hand, due to the oil crisis, this has brought the companies to use heavy oils with very high viscosities and thus to emulsify them to reduce their viscosity for transport in pipes. This interest for oil emulsions decreased greatly the last years but found a renewed success with the development of new crude-oil production drilling techniques using inverse emulsion mud and with appearance of secondary oil recovery techniques using micro-emulsions.

II. Emulsion Characteristics

Emulsion is generally defined as colloidal systems in which the interfacial tension between the two phases is large enough for the dispersed particles to have a spherical shape at rest.

This gives a close analogy between deformable particles suspensions and emulsions rheological behaviours. One of the differences between them is the existence of two different types of emulsions made from the two same phases: oil-in-water or water-in-oil emulsions, these two types depend from the respective oil concentrations and from the emulsifier properties.

Like for solid suspensions, the rheological behaviour of an emulsion may depend from the two phase's properties: concentration of the dispersed phase, granulometry and size of the particles, Newtonian or non-Newtonian behaviour of the liquids.

Moreover, for a given type of two given emulsions, direct or inverse, a limit concentration of the dispersed phase may exist and correspond to a maximum "packing" of the droplets. For mono-disperse size distribution of the spherical particles, this limit is around 65% and would be slightly higher when the particles are deformable. Higher oil concentrations will bring either to inversion or to separation of the phases.

The range between 25% and 75% corresponds, in theory, to a region where direct and inverse emulsions of two emulsions can exist. Experimental results reported by Becher [1] have showed that the oil concentration at inversion depends of the emulsifier concentration.

A third type of emulsions was also observed by Mao and Mardsen [2], an oil-in-water-in-oil emulsion corresponding to inclusion of small oil droplets in the water droplets dispersed in the oil phase.

III. Rheological Models

Among the models proposed to explain the concentration dependence of the viscosity it is obvious to refer to Einstein's work considering the influence of spherical dispersed particles on the viscosity of a liquid even if this model is only valid for very dilute and rigid suspensions. About thirty years later Taylor [3] proposed a model in which he considered the particles as spherical but deformable and that the circulation of the liquid inside the droplet brings to less dissipation of energy.

Manuscript received and revised April 2014, accepted May 2014

The next significant progress were made during the fifties by Oldroyd [4] who modified the Taylor model in taking into account the interfacial absorption layer of the particles. Several other attempts were made to include other effects like electro-viscous or particle dimension effects.

On the other hand, Mooney [5] proposed an exponential model similar to that developed by Richardson [6] for deformable suspensions. These models, based on experimental observations, fit generally well the data for concentrations lower than 60%. Camy and al. [7] have confirmed that the viscosity of crude oil emulsions is related to the oil concentration by an exponential relationship:

$$\frac{\eta}{\eta_0} = exp(KC) \tag{1}$$

where:
- η = viscosity of emulsion
- η_0 = viscosity of the continuous phase
- K = coefficient
- C = oil concentration

One of the failures of these models is that they cannot predict the shear dependency of the viscosity. Like for solid suspension a shear thinning rheological behaviour is generally observed if the oil concentration is high enough. Simple models, like Ostwald power-law are generally used to describe this behaviour with more or less success. A model was proposed by Quemada [8] and used successfully for crude oil emulsions. This model has the particularity in combining the concentration and shear effects through the definition of an intrinsic viscosity shear dependent:

$$\frac{\eta}{\eta_0} = \left(1 - \frac{1}{2} KC\right)^{-2} \tag{2}$$

where:
- $K = f(C, D)$: intrinsic generalized viscosity
- D = shear rate

IV. Experimental Procedure

The purpose of this work was to study the effect of oil concentration on the viscosity of the mixture and thus the effect of the emulsifier concentration was not taken into account here: this concentration was kept constant for a given oil-water pair. Most part of the measurements was performed with a commercial lubricant emulsion used in mechanical industry for lubrication of drilling and cutting tools. Measurements were also performed with emulsions of heavy crude oil in water. The oil phase viscosity was found to be Newtonian for the lubricant and shear-thinning for crude oil. A microscope with camera (Photo A) was used to observe the mixture of the crude oil emulsion.

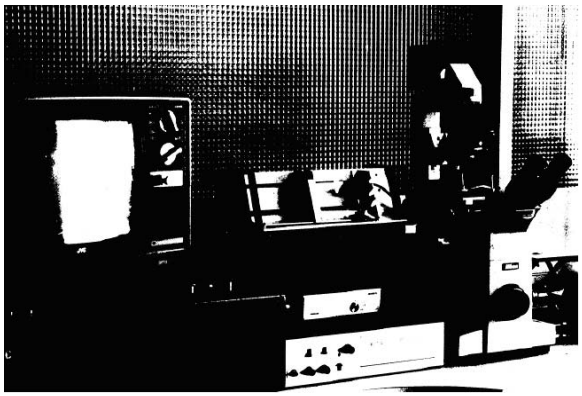

Photo A. Microscope with camera

Figs. 1 show microscope-pictures of crude oil-and-water emulsions at increasing oil concentrations. The third picture (Fig. 1(c)) corresponds to 75% of crude oil. This concentration was found to be the limit where the mixture inverts spontaneously. On this figure, one can observe that the large droplets remain in touch without collapse and that the interfacial surface between two particles is increased by deformation of the droplets. The pores between these large droplets are filled with smaller scale droplets.

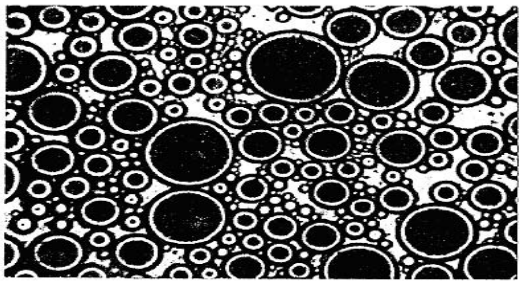

(a)

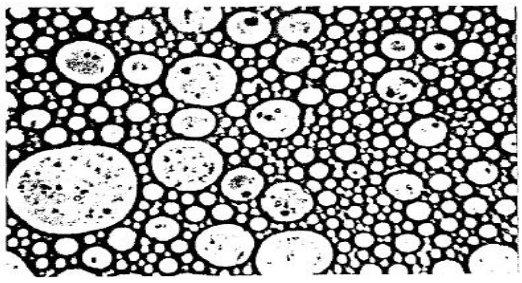

(b)

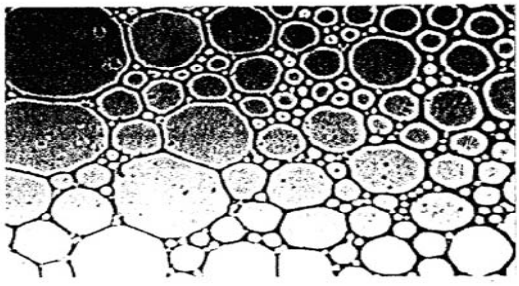

(c)

Figs. 1. Photographs of the internal structure of crude oil emulsions

The crude oil emulsions were prepared by mixing oil and distilled water in which the emulsifier (2% of Cemulsol) was previously added. A conventional screw mixer was used to prepare the mixtures. The emulsions were permanently agitated before use.

The lubricant oil contains itself the emulsifier and it was just necessary to add the volume of water to obtain a homogeneous emulsion except for high oil concentrations where gentle agitation was necessary to mix the two phases.

A commercial rotating cylinder viscosimeter (Photo B) was used to measure the stress-strain relations and the viscosity. Most of our measurements were made with a double gap rotating cylinder (NV St) to increase the sensibility of the system.

Photo B: Rotovisko Haake RV 2

The gap width has about 0.4 mm and is small enough to reduce the problems of data corrections for measurements of non-Newtonian mixtures and large enough in regard to the dimensions of the largest droplets (40 micrometers). It is to be noted that the slip at wall that has indicated by Barnes [9] was not taken into account in the present work.

V. Experimental Results

V.1. Strain-Stress Evolution

Evolution of the shear stress versus the shear rate for the lubricant emulsion is presented in Fig. 2 for oil concentrations ranging between 10% and 100%. One can observe that the rheological behaviour is Newtonian for pure oil and not far from Newtonian for the very low concentrations (10% and 20%). Between 20% and 70% the shear thinning non-Newtonian behaviour increases progressively.

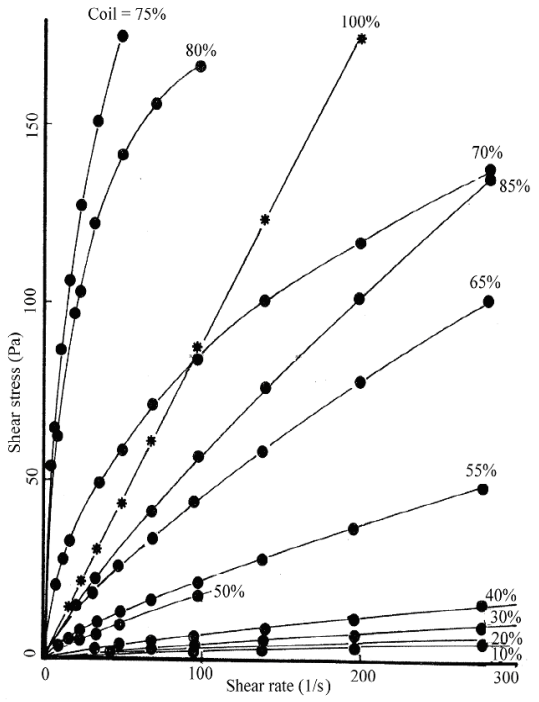

Fig. 2. Evolution of the flow curves of cutting oil emulsions with concentration

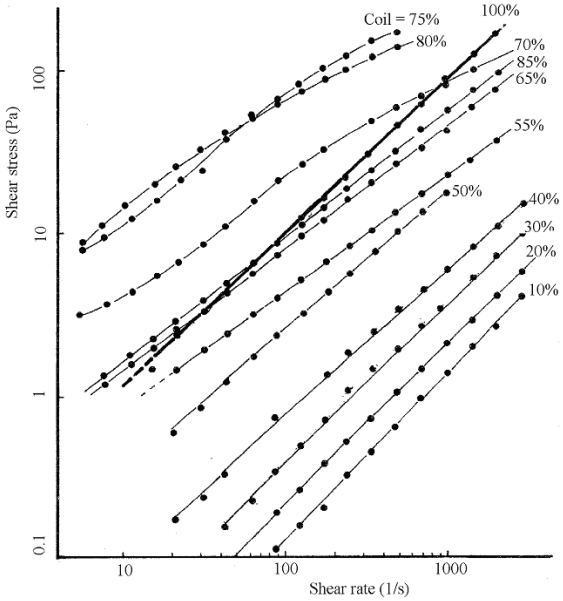

Fig. 3. Logarithmic plot of the evolution of the flow curves with concentration

An important jump is than observed between 70% and 75% followed by a decrease at 80% and 85%.

The logarithmic plot of the data (Fig. 3) confirms the change of behaviour at an oil concentration near from 70%. Until 70% the evolution of the log-log curves is linear with a slope less than 1 and the rheological behaviour can be represented by Oswald's power-law model with a good approximation in the range of explored shear rates. Fig. 4 shows the evolution of the fluid rheological index and consistency.

In the oil concentration range from 10% to 30% the fluid index is close to 1 and, in regard to the plot of Figs. 2 and 3 one can expect that the mixture behaves like a Binghamian fluid with a weak yield stress. At higher oil concentrations the evolution of the shear stress versus the shear rate is no more linear.

The effect of the shear rate on the structure of the mixture seems to become important in this range of concentration probably related to agglomeration, coalescence and emulsion inversion. At oil concentration higher than 80% the power law evolution is found again. Yasushi and Clive [8] have showed at high oil concentrations emulsions exhibit high elasticity due to formation of planar films between droplets.

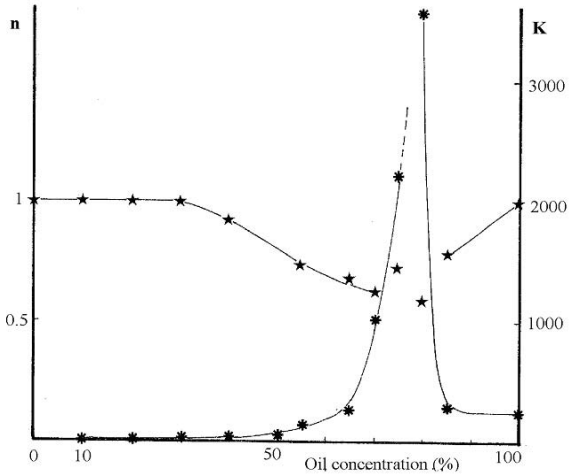

Fig. 4. Variation of the fluid index and the consistency with concentration

V.2. Influence of Concentration on the Viscosity

The apparent viscosity, deduced from the previous data, is represented versus oil concentration on a semi-logarithmic plot in Fig. 5 for different shear rates. An important peak of viscosity is observed at the oil concentrations ranging between 70% and 80%. Woelflin [11] have showed the same result for crude oil emulsion.

At the highest shear rates (3000 sec^{-1}); the viscosity is more than 15 times higher than the viscosity of oil alone.

This peak was previously observed by Mao and Mardsen [2] for crude oil emulsions. The semi-logarithmic representation shows also that the exponential models of viscosity-concentration evolution based on Richardson's work [6] are only valid in a range of oil concentrations different for each shear rate.

This divergence has been previously noted by Mao and Mardsen [2] for low oil concentrations.

The divergence with an exponential model increases greatly at low shear rates and remains valid only in a small domain of oil concentrations near the critical concentration at very low shear rates (10 s^{-1}).

For oil concentrations above 80% the viscosity decreases when oil concentration increases but, due to the few number of measurements any conclusion can be taken concerning the use of an exponential model.

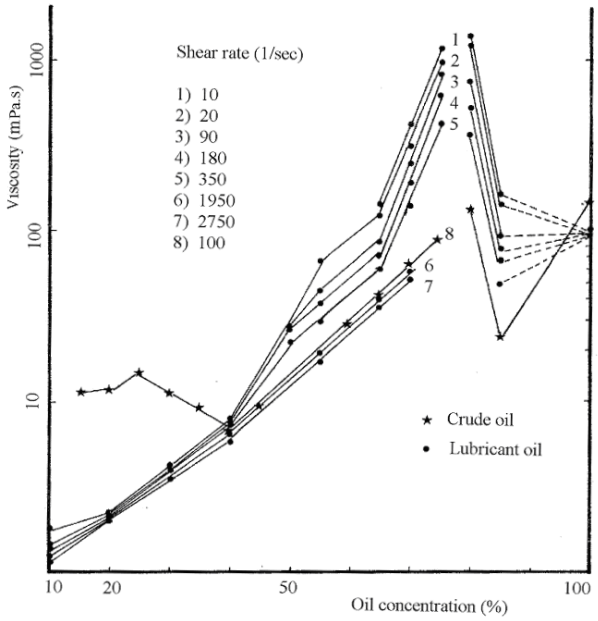

Fig. 5. Variation of the viscosity with concentration at different shear rate

It can be noted that the viscosity is lower than the pure oil viscosity at high shear rates and an oil concentration of 85%.

Similar results were obtained with crude oil emulsions and particularly the existence of a peak of viscosity at a concentration around 75% (Fig. 5). The major differences were observed at low oil concentration where an unexplained second peak was observed.

We can conclude that the results obtained, in particular, the inversion of phases as well as the peak of viscosity are phenomenon which characterize the majority of the emulsions derived from oil industry.

VI. Conclusion

The results obtained with two different oil emulsions have showed the increase of viscosity with oil concentration until a critical concentration. Visual observation of the emulsion has showed that this critical point corresponds to an inversion of the emulsion. The evolution of the viscosity with oil concentration at a given shear rate cannot be represented by an exponential relationship as proposed by several authors except at high shear rates in an oil concentration range close to the peak of viscosity.

This behaviour can probably be explained by a change in structure of the emulsion (coalescence or agglomeration of the particles) at the lower shear rates. It is difficult to confirm this hypothesis without a control of the emulsion granulometry during the test.

The drastic increase of viscosity near the critical oil concentration can have important consequences for lubrication industrial applications where the emulsions are recycled during several hours and can change of properties by evaporation of water.

References

[1] P, Becher, *Emulsions: Theory and Pratice* (New York: 2nd ed., Reinhold Publishing Corporation, 1965).

[2] M.L Mao, S.S. Mardsen, Stability of concentrated crude oil-in-water emulsions as a function of shear rate, temperature and oil concentration, *J. of Canadian Petroleum Techn*. Vol.54**,** pp. 04-06, 1977.

[3] G.I. Taylor, The viscosity of a fluid containing small drops of another fluid, *Proc. Royal Soc. London Ser*., A138, 1932, pp.41.

[4] J.G. Oldroyd, The effect of interfacial stabilising films on the elastic and viscous properties of emulsions, *Proc. Royal Soc*., A232**,** 1955, pp.567.

[5] Mooney, M. (1951). *Journal of Colloid. Sci.* **6** : 162

[6] E., G. Richardson, The flow of emulsions, *J. Colloid Sci*., Vol. 8, pp.367, 1958.

[7] Camy, J.P. and al. (1975). *Proc. 2nd Int. Symp. on Oilfield Chem.* Dallas : SPE 5299

[8] D, Quemada, Rheology of concentrated disperse s ystems, II. A model for non-Newtonian shear viscosity in steady flows, *Rheologica Acta*, Part II, Vol.17**,** pp.63, 1978.

[9] H. A. Barnes, A review of the slip (wall depletion) of polymer solutions, emulsions and particle suspensions in viscosimeters: its cause, character and cure, *J. Non-Newtonian Fluid Mech*. Vol.56, pp.221, 1995.

[10] S. Yasushi, and A.P. Clive, Droplet deformability and emulsion rheology: steady and dynamic behavior, *Korea-Australia Rheology Journal*, Vol. 17, N° 4, pp.191-198, 2005.

[11] Woelflin, W. The viscosity of crude oil emulsions. *Presented at Spring Meeting*, Los Angeles, California, march 10, 1942, 148-153.

Authors' information

Faculté de Génie Mécanique, Université des Sciences et de la Technologie Mohamed Boudiaf d'Oran. B.P. 1505 Oran El Ménouar – 31000 Oran – Algérie

E-mail : benali_lar@yahoo.fr

2035-1763(201405)6:3;1-5